博士論文

Classic cadherins mediate selective intracortical circuit formation in the mouse neocortex

（細胞接着分子カドヘリンを介した

マウス大脳皮質局所回路の形成機構解析）

脇元　麻有

Table of Contents

Abstract

Understanding the molecular mechanisms underlying the formation of selective intracortical circuitry is one of the important questions in neuroscience research. "Barrel nets" are recently identified intracortical axonal trajectories derived from layer 2/3 neurons in layer 4 of the primary somatosensory (barrel) cortex. Axons of layer 2/3 neurons are preferentially distributed in the septal regions of layer 4 of the barrel cortex, where they show whisker-related patterns. Because cadherins have been viewed as potential candidates that mediate the formation of selective neuronal circuits, here I examined the role of cadherins in the formation of barrel nets. I disrupted the function of cadherins by expressing dominant-negative cadherin (dn-cadherin) using *in utero* electroporation and found that barrel nets were severely disrupted. Confocal microscopic analysis revealed that expression of dn-cadherin reduced the density of axons in septal regions in layer 4 of the barrel cortex. I also found that cadherins were important for the formation, rather than the maintenance, of barrel nets. My results uncover an important role of cadherins in the formation of local intracortical circuitry in the neocortex.

Introduction

The cerebral cortex contains complex and sophisticated neuronal circuitries that are the structural bases of higher brain functions. Because the formation of appropriate neuronal circuitry in the cerebral cortex during development is essential for normal brain functions, it is important to elucidate the mechanisms underlying the formation of neuronal circuitry in the cerebral cortex. Although previous electrophysiological and anatomical studies have well revealed the cortical circuitry in the cerebral cortex, the molecular mechanisms underlying the formation of intracortical circuits during development are not fully understood[1,2].

One of major difficulties has been that, until recently, there have been few feasible models to study intracortical circuit formation compared to other systems. The rodent somatosensory (barrel) cortex has widely served as a model system because of the existence of "barrels" in its layer 4 (Fig. 1) [1]. Since barrels have evident patterns in layer 4 that corresponds to the pattern of whiskers, and because barrels are readily identifiable using common histological techniques, they have been serving a great deal to reveal cortical pattern formation and cortical afferent development [3-14]. Thus, a model system that allows easy visualization of the reproducible circuit pattern would be a prerequisite in facilitating the study of selective intracortical circuit formation.

To elucidate the molecular mechanisms of selective intracortical circuit formation, I used "barrel nets" in the mouse barrel cortex as a model in this study. Barrel nets refer to a spatial pattern of axons found in layer 4 of the barrel cortex; axons of layer 2/3 neurons are predominantly located in septal regions (i.e., regions between barrels) of layer 4 and therefore show a whisker-related pattern (Fig. 2) [15-17]. There are presynaptic structures on barrel nets, implying that barrel nets are involved in the

functioning of the neuronal circuitry of the barrel cortex [15,16]. Importantly, it can be easily visualized using *in utero* electroporation, which can be used for genetic perturbations at the same time. Therefore, I considered the pattern of barrel nets to be a good model for investigating the mechanisms of selective intracortical circuit formation.

To investigate the molecular mechanisms underlying the pattern formation of barrel nets, I focused on classic cadherins, which are known as homophilic cell adhesion molecules [18-21]. This was because it has been proposed that the homophilic binding activity of classic cadherins is well suited to mediate selective circuit formation [22,23]. Furthermore, it has been reported that several classic cadherins are predominantly expressed in whisker-related patterns in the barrel cortex. For example, *cadherin-8* mRNA was detected in septal regions of layer 4, as well as layers 2/3 and 5a [22,24-28]. Previous studies showed that, in the developing barrel cortex, *cadherin-6* expression is relatively high in septal regions compared with barrel hollows [22,26,27,29,30]. Immunohistochemical studies revealed that R-cadherin and N-cadherin expressions are observed in barrel hollows of layer 4 [31,32]. In addition, a broad range of classic cadherins, including *cedherin-7, 9, 10, 11, 12, 14, 19, 20, 22, 24*, are known to be expressed in the developing barrel cortex with different spatiotemporal specificities [27]. Although the existence of whisker-related patterns is yet to be tested for the expression patterns of these cadherins, it is plausible that at least some of them are expressed differently between barrel and septal regions in layer 4. Therefore, it seemed plausible that classic cadherins are involved in the pattern formation of barrel nets. However, the roles of classic cadherins in selective circuit formation in the cerebral cortex still remained largely elusive. Although numerous classic cadherins are expressed in the neocortex, no defect in intracortical circuits formation has been reported. This could be because

various cadherins work redundantly in the developing neocortex, and knocking out only one subtype of cadherin is not sufficient for disrupting intracortical circuit formation [33]. Therefore, I used dominant-negative cadherin (dn-cadherin) in order to suppress the function of multiple classic cadherins simultaneously in this study. Using *in utero* electroporation, I suppressed cadherin function in region- and layer-specific manners. Here, using barrel nets as a model, I uncovered a role of classic cadherins in intracortical circuit formation.

Materials and Methods

Animals

ICR mice were purchased from SLC (Hamamatsu, Japan) and were reared on a normal 12 h light/dark schedule. The day of conception and that of birth were counted as E0 and P0, respectively. All procedures were performed in accordance with protocols approved by the University of Tokyo Animal Care Committee and Kanazawa University Animal Care Committee. All experiments were repeated at least three times and gave consistent results.

Plasmids

All genes were expressed under the control of the CAG promoter [34]. Plasmids were purified using the EndoFree plasmid maxi kit (QIAGEN, Germany). pCAG-GFP, pCAG-mCherry and pCAG-synaptophysin-GFP were described previously [16]. Dominant-negative cadherins, hDNcad and cN390Δ, were generous gifts from Dr. Jonas Frisén (Karolinska Institutet, Sweden) and Dr. Masatoshi Takeichi (RIKEN CDB, Japan), respectively [35-38]. pCAG-hDNcad and pCAG-cN390Δ were made by substituting GFP of pCAG-GFP with hDNcad and cN390Δ, respectively. pCAG-synaptophysin-mCherry was made by substituting GFP of pCAG-synaptophysin-GFP with mCherry. pCAG-ER^{T2}CreER^{T2} and pCAG-floxedSTOP-GFP were described previously [39]. pCAG-floxedSTOP-mCherry, pCAG-floxedSTOP-hDNcad and pCAG-floxedSTOP-cN390Δ were made by replacing GFP of pCAG-floxedSTOP-GFP with mCherry, hDNcad and cN390Δ, respectively.

In utero *electroporation*

In utero electroporation was performed as described previously with slight modifications [16,40,41]. Briefly, pregnant animals were anesthetized with sodium pentobarbital, and the uterine horns were exposed. Approximately 1-2 μl of DNA solution (1-3 mg/ml) was injected into the lateral ventricle of embryos at the indicated ages using a pulled glass micropipette. Each embryo within the uterus was placed between tweezer-type electrodes (CUY650-P5, NEPA Gene, Japan). Square electric pulses (45 V, 50 ms) were passed 5 times at 1-s intervals using an electroporator (ECM830, Harvard Apparatus, USA). The directions of pulses were adjusted so that cortical glutamatergic neurons were transfected. Care was taken to quickly place embryos back into the abdominal cavity to avoid excessive temperature loss. The wall and skin of the abdominal cavity were sutured, and embryos were allowed to develop normally.

4-Hydroxytamoxifen administration

4-Hydroxytamoxifen (4-OHT) (>70% Z isomer, Sigma-Aldrich, USA) administration was performed as described previously with slight modifications [39]. 4-OHT was dissolved in 99.5% EtOH at a concentration of 20 mg/ml as stock solution. The stock solution was diluted with sesame oil at a concentration of 2 mg/ml before use, and then, the EtOH was vaporized. 4-OHT in sesame oil was injected subcutaneously 66 μg/g of body weight at the indicated time points.

Dissociated primary cultures of cortical neurons

Cultures of dissociated cortical neurons were made as described previously with slight modifications [42]. *In utero* electroporation was performed at E15.5, and the cerebral

cortex was dissected at E16.5. After the meninges were pulled off, the dissected cortices were incubated for 20 min in papain solution plus DNase I at 37°C, and were dissociated mechanically. The dissociated neurons were plated onto poly-D-lysine-coated coverslips in 24-well plate ($1x10^6$ cells/well), and maintained in 50% Basal Medium Eagle (Invitrogen, USA) containing 1 mM L-glutamine (Sigma-Aldrich), 25% Hank's balanced salt solution (Invitrogen), 25% horse serum (Invitrogen), 6.5 mg/ml D-glucose (Sigma-Aldrich), 100 U/ml penicillin/streptomycin (Invitrogen), and 1% HEPES pH 7.4 (Invitrogen) at 37°C in 5% CO_2. The day of dissection was counted as day *in vitro* 0 (DIV0).

Immunohistochemistry and immunocytochemistry

Immunohistochemistry was performed as described previously [11,43,44]. Briefly, mice were anesthetized with pentobarbital and transcardially perfused with 4% paraformaldehyde/PBS. To make coronal sections, the cerebral cortices were dissected, cryoprotected by overnight immersion in 30% sucrose/PBS, and embedded in OCT compound. To make tangential sections, the cortical hemispheres were isolated, flattened and embedded in OCT compound as described previously [11,16]. Sections were made using a cryostat.

Sections of 50 μm thickness were permeabilized with 0.1–0.5% Triton X-100 in PBS and incubated overnight with primary antibodies. After being incubated with Alexa 488-, Alexa 647- or Cy3- conjugated secondary antibodies and 1 μg/ml Hoechst 33342, the sections were washed and mounted. The primary antibodies included rabbit anti-VGLUT2 antibody (Synaptic Systems, Germany), goat anti-VGLUT2 antibody (Frontier Institute, Japan), rabbit anti-GFP antibody (Medical & Biological Laboratories,

Japan), rat anti-GFP antibody (Nacalai Tesque, Japan), rabbit anti-RFP antibody (Medical & Biological Laboratories, Japan), rabbit anti-RORβ antibody (Diagenode, USA), goat anti-Brn2 antibody (Santa Cruz, USA), and rat anti-Ctip2 antibody (Abcam, USA).

For immunocytochemistry, dissociated neurons cultured on coverslips were fixed with 4% paraformaldehyde/PBS for 15 min at 37°C. Then, the neurons were incubated in blocking solution (2% BSA/PBS), and were incubated at 4°C overnight with primary antibodies, which included rat anti-GFP antibody (Nacalai Tesque) and sheep anti-N-cadherin antibody (R&D Systems, USA). The neurons were washed with 0.5% Triton X-100/PBS and then incubated with Alexa488- and Cy3-conjugated secondary antibodies and 1 μg/ml Hoechst 33342, followed by washing and mounting.

In situ *hybridization*

In situ hybridization was performed as described previously with slight modifications [45,46]. Sections with 25 μm thickness were prepared from fresh-frozen tissues, and those with 14 μm thickness were from fixed tissues. The sections were treated with 4% paraformaldehyde for 10 min and 0.25% acetic anhydride for 10 min. After prehybridization, the sections were incubated overnight at 58°C with digoxigenin-labeled RNA probes for *cadherin-6*, *cadherin-8* or *hDNcad* diluted in hybridization buffer (50% formamide, 5×SSC, 5×Denhardt's solution, 0.3 mg/ml yeast RNA, 0.1 mg/ml herring sperm DNA, and 1 mM DTT). The sections were washed with SSC, incubated with alkaline phosphatase-conjugated anti-digoxigenin antibody (Roche, Switzerland), and then incubated with NBT/BCIP as substrates.

In some experiments, VGLUT2 immunohistochemistry was performed after *in*

situ hybridization for *cadherin-6* and *cadherin-8*. Immunohistochemistry was performed as described.

Microscopy

Epifluorescence microscopy was performed with an AxioImager A1 microscope (Carl Zeiss, Germany) or a BIOREVO BZ-9000 (Keyence, Japan). Confocal microscopy was performed with an LSM510 microscope (Carl Zeiss) or an FV10i FLUOVIEW microscope (OLYMPUS, Japan).

Quantifications of barrel net formation

Quantifying GFP fluorescence of barrel nets was performed as described previously [16]. Briefly, coronal sections of 50 μm thickness were prepared at the indicated time points and stained using VGLUT2 antibody. Sections containing posterior regions of the barrel cortex were used. Images were taken under a confocal microscope. Regions of interest (ROIs) in layer 4 were selected as rectangular areas of 50 μm heights so that the edges of VGLUT2-positive TCA patches could most clearly be seen. Signals in ROIs were then measured using the "Plot Profile" command of ImageJ (NIH). Each barrel unit (which refers to a barrel and its septal rim) was then separated using VGLUT2 signal intensities in layer 4. GFP signals within each barrel unit were normalized by subtracting the minimum value within the barrel unit from the measured values, and dividing the values by the total signal intensity of the barrel unit. Each barrel unit was divided into ten subunits of equal width (hereafter referred to as barrel subunits), and the values of each subunit were plotted against the horizontal position of the subunit within the barrel unit.

To calculate the periphery/center ratio (p/c ratio) for GFP, the mean signal intensity of subunits 1 and 10 was divided by that of subunits 5 and 6. The center/periphery ratio (c/p ratio) of VGLUT2 was the inverse number of the p/c ratio. For statistical analyses of the p/c and c/p ratio, the average value was calculated for each pup and compared using Welch's *t*-test.

Quantification of the morphology of dissociated neurons

Dissociated primary cultures were fixed at DIV4 and were stained with anti-GFP antibody. Images were taken under an epifluorescence microscope, and axons from individual neurons were traced using the NeuronJ plugin [47,48] of ImageJ software. I used the "Add tracings" command for tracing the axons and the "Measure tracings" command for measuring the length of axon branches in NeuronJ. Branch patterns were annotated manually using NeuronJ, and then the analysis and statistics were performed using the R environment [49]. Five GFP-positive neurons on each coverslip were traced and analyzed. Seven coverslips per each experimental condition were used for statistical analyses using Welch's *t*-test.

Quantifications of the expression of layer markers and the density of GFP-positive neurons

Z-stack images of immunostained sections were taken using a confocal microscope, and the expression of layer markers was examined in GFP-positive neurons with Hoechst-positive nuclei. GFP-positive neurons without Hoechst-positive nuclei were excluded from the analyses.

To determine the transfection efficiency, the density of GFP-positive neurons in layer 2/3 of coronal sections with 50-μm thickness was calculated. Statistical analyses were performed using Mann-Whitney's *U*-test.

Quantifications of the density and the size of synaptophysin-mCherry-postive puncta

Coronal sections prepared at P15 were immunostained, and *Z*-stack confocal images were taken at the pixel resolution of 0.041 μm for X and Y axes. Average-projection images with 3.5 μm optical thickness were smoothened (mean filter, 2 μm radius) and then used for further analyses. Synaptophysin-mCherry positive puncta were detected using the "Find maxima" command of ImageJ, in which mean plus standard deviation values were used as the tolerance level. GFP-positive axons were traced, and their lengths were measured using the original images and NeuronJ. Then, mCherry-positive puncta were counted only if they overlapped with GFP-positive axons. The radius of mCherry-positive puncta was calculated as the distance from the maxima to the first deflection point of the mCherry fluorescence. Mann-Whitney's *U*-test was used for statistical analyses.

Results

ER^{T2}Cre-mediated postnatal expression of dominant-negative cadherin in layer 2/3 neurons

Because it has been reported that the multiple classic cadherins are expressed in whisker-related patterns in the somatosensory cortex (Fig. 3) [26,28,31,32,50], I simultaneously suppressed functions of multiple classic cadherins using dn-cadherin. In this study, I mainly used a dn-cadherin called hDNcad [35,36]. hDNcad is the membrane-tethered cytosolic protein which is comprised of solely from the intracellular domain of human N-cadherin [35,36]. It was reported that hDNcad suppressed the functions of various classic cadherins by facilitating their protein degradation [35]. Consistent with a previous report [35], my experiments using dissociated primary cultures of the cerebral cortex demonstrated that hDNcad strongly inhibited the expression of classic cadherins in cortical layer 2/3 neurons (Fig. 4). I then co-expressed GFP and hDNcad in layer 2/3 neurons *in vivo* using *in utero* electroporation at E15.5 under the control of the CAG promoter. Consistent with a previous report [51], however, constitutive expression of hDNcad disrupted migration of the GFP-positive transfected layer 2/3 neurons (Fig. 5*A*).

To avoid the migration defects caused by dn-cadherin, I used the ER^{T2}Cre/loxP system to control the timing of dn-cadherin expression (Fig. 5*B*) [52]. I transfected layer 2/3 neurons with pCAG-ER^{T2}CreER^{T2}, pCAG-floxedSTOP-XFP and pCAG-floxedSTOP-hDNcad using *in utero* electroporation at E15.5 and examined the time point after which 4-OHT injection does not lead to the migration defect (Fig. 5*B*, *C*). While injection of 4-OHT at P0 caused the evident migration defect (Fig. 5*C*, arrowheads), injection at or after P2 did not (Fig. 5*C*). I therefore injected 4-OHT at P2

in the following experiments.

Next, I examined how many times of 4-OHT injection are necessary for sufficient ER^{T2}Cre-mediated gene expression (Fig. 6). Expression levels of GFP and the number of GFP-positive cells were markedly increased in samples that received 4-OHT injection daily for three consecutive days than in those that received injection only once (Fig. 6*B*). Therefore, to sufficiently express dn-cadherin only after migration of layer 2/3 neurons had occurred, I injected 4-OHT daily from P2 to P4 in the following experiments.

Postnatal expression of dn-cadherin in layer 2/3 neurons disrupted barrel nets in the barrel cortex

I then examined whether classic cadherins are required for the formation of barrel nets by expressing dn-cadherin and GFP in layer 2/3 neurons (Fig. 7*A*). Although the whisker-related pattern of barrel nets was clearly visible in tangential sections of control samples, I found that the pattern was almost absent in samples expressing hDNcad (Fig. 7*B*). To make sure that this effect of hDNcad is mediated by suppressing cadherin functions, I employed another dn-cadherin, cN390Δ [37,38]. cN390Δ is made by deleting a large fraction of the extracellular domain of chick N-cadherin [37]. It was reported that cN390Δ competed with endogenous cadherins, and thereby suppressed their functions [37,38]. I found that the expression of cN390Δ also resulted in disruption of barrel nets (Fig. 7*C*), indicating that the phenotype of hDNcad was indeed the result of suppressing cadherin functions. Examination using coronal sections also showed that GFP-positive axons failed to accumulate in septal regions of layer 4 when one of the dn-cadherin constructs was expressed in layer 2/3 (Fig. 8*A*, hDNcad and cN390Δ). These results

suggest that inhibition of classic cadherin functions in layer 2/3 neurons disrupts the formation of the barrel net pattern.

I then quantified the effect of dn-cadherin on barrel net formation with a method we used previously [16]. I quantified the distribution of GFP-positive axons around individual barrels in coronal sections using confocal microscopic images (Fig. 8*B*). In control samples, GFP-positive axons were abundant in peripheral regions around thalamocortical axon patches visualized by anti-VGLUT2 antibody (Fig. 8*B*, control; compare green and gray) [53,54]. In contrast, in dn-cadherin samples, such preferential distribution of GFP-positive axons was inhibited (Fig. 8*B*, hDNcad, green). I calculated the ratio of GFP signal intensities in peripheral regions to those in central regions of individual VGLUT2-positive patches (hereafter referred to as "the periphery/center ratio" or "the p/c ratio," see Materials and Methods for details) (Fig. 8*C*, green). I found that the p/c ratio of GFP was significantly higher in control samples than that in dn-cadherin samples (Fig. 8*C*, green), whereas the c/p ratio of VGLUT2 signals was similar in both control and dn-cadherin samples (Fig. 8*C*, gray) (n = 3 pups for each condition from 3 pregnant mice. 34 barrel units from control samples and 45 barrel units from hDNcad samples). However, the density of GFP-positive layer 2/3 neurons in hDNcad samples was not different from that in control samples (Fig. 8*D*) (n = 3 pups for each condition from 3 pregnant mice). Taken together, these results indicate that classic cadherins play a crucial role in the formation of barrel nets.

Classic cadherins are required for the accumulation of fine axons in septal regions

Because our previous confocal microscopic studies showed that there is a much higher density of GFP-positive fine axon branches in septa than in barrel hollows [15,16], it

seemed plausible that the effect of dn-cadherin on barrel nets resulted from the reduction of fine axons in the septal regions of layer 4. I therefore examined the phenotype of dn-cadherin overexpression in more detail using a confocal microscope (Fig. 8*E*). I found that the number of fine axon branches markedly decreased in septal regions when hDNcad was expressed (Fig. 8*E*). Although hDNcad samples may have more axons in the barrel hollows, it was difficult to conclude whether hDNcad affected the number of axons in the barrel hollows. These results indicate that classic cadherins are required for the accumulation of fine axons in the septal regions of layer 4.

Because previous studies reported that classic cadherins are involved in axonal elongation of retinal ganglion cells [55], it was possible that the effect of dn-cadherin on barrel nets was just a result of a general defect in the axonal elongation of transfected layer 2/3 neurons. In order to address whether dn-cadherin expression affects axon elongation in general, I examined the extent of callosal axon projection from layer 2/3 neurons (Fig. 9). Notably, layer 2/3 neurons, regardless of whether they were transfected with hDNcad or control vectors, sent callosal axons to a similar extent in the contralateral cortex, suggesting that the defect in the formation of barrel nets in dn-cadherin samples is not simply because of the inhibition of axonal elongation in general.

It seemed intriguing to examine the effects of dn-cadherin on the morphology of the axons of layer 2/3 neurons at the single-cell level. I therefore transfected layer 2/3 neurons with pCAG-GFP plus either pCAG-hDNcad or a control plasmid, and made dissociated primary cultures of the cerebral cortex (Fig. 10). Although I quantified several parameters of the morphology of axons such as the number of branches per an axon (Fig. 10*B*), the total length of each axon (Fig. 10*C*) and the length of individual

axonal branches (Fig. 10*D*, *E*), none of these parameters were significantly different between control and hDNcad-transfected neurons (n = 7 coverslips for each condition). These results imply that dn-cadherin affects the location of axonal branches but not the branching or elongation of axons.

Although dn-cadherin-expressing layer 2/3 neurons were located in the appropriate layer (i.e., layer 2/3), it seemed still possible that the expression of dn-cadherin affected the layer identities of transfected layer 2/3 neurons, and as a result, the pattern of barrel nets was disrupted. To address this point, I performed immunohistochemistry using antibodies against layer marker proteins (Fig. 11). I used Brn2, which is predominantly expressed in layers 2/3 and 5, and Ctip2, which is a marker for layers 5–6 [56,57]. I also used RORβ, which is mainly expressed in layer 4 and sparsely in layer 5 [58,59]. Higher magnification images showed that Brn2, RORβ and Ctip2 immunoreactivities were located in the nucleus (Fig. 11*D, E*). I found that expression patterns of the layer markers in hDNcad samples were indistinguishable from those in the control samples (Fig. 11*A*-*C*). In addition, my quantification also revealed that GFP-positive cells in the hDNcad samples had similar expression profiles to those in control samples (Fig. 11*C*; n = 3 pups for each condition from 5 pregnant mice). These data suggest that postnatal overexpression of dn-cadherin does not affect the layer identities of transfected layer 2/3 neurons but specifically alters the regional selectivity of axon distribution in layer 4 of the barrel cortex.

Postnatal dn-cadherin expression decreased presynaptic structures in septal regions

Because our previous studies have suggested that barrel nets contain presynaptic structures [15,16], I next examined whether the expression of dn-cadherin affects the

number of synaptic structures on barrel nets. I examined the distribution of presynaptic structures on barrel nets, using XFP-tagged synaptophysin as a presynaptic marker [15,16].

First, I examined the developmental time course of the formation of presynaptic structures on barrel nets. I expressed mCherry and synaptophysin-GFP in layer 2/3 neurons and examined the distribution patterns of GFP-positive puncta on mCherry-positive barrel nets during development (Fig. 12*A*). Synaptophysin-GFP-positive puncta markedly increased between P5 and P15, corresponding to the increase of mCherry-positive axons in septal regions (Fig. 12*A*). I found that the number of synaptophysin-mCherry puncta was markedly reduced by hDNcad, suggesting that dn-cadherin expression affects not only the distribution of axons but also the number of presynaptic structures on barrel nets (Fig. 12*B*). My quantification of mCherry-positive puncta on GFP-positive axons showed that neither their density (i.e., the number of mCherry-positive puncta per unit axon length) nor the size of individual mCherry-positive puncta was affected by hDNcad expression (Fig. 12*C*-*E*; n = 3 pups for each condition from 4 pregnant mice). This result suggests that although the number of mCherry-positive puncta was reduced by hDNcad, this reduction is due to the decrease in the number of axons in the septal region.

Classic cadherins are required for the formation, but not for the maintenance, of barrel nets

So far, my results were consistent with the idea that classic cadherins are required for the formation of barrel nets. On the other hand, it still remained possible that classic cadherins are involved in the maintenance, rather than the formation, of the pattern of barrel nets. However, I believe that this is unlikely because of the following two reasons.

The first reason is that barrel nets did not appear from the beginning when dn-cadherin was expressed. I examined the effect of hDNcad sequentially at P5, P10 and P15 (Fig. 13*A*). In control animals, barrel nets were invisible at P5 and were formed gradually thereafter as we reported previously [16]. Interestingly, in hDNcad-transfected animals, barrel nets never appeared (Fig. 13*B*), suggesting that the formation of barrel nets was inhibited.

The second reason is the fact that expression of dn-cadherin after the formation of barrel nets did not disrupt barrel net patterns. I expressed hDNcad after the formation of barrel nets by late administration of 4-OHT and examined whether the late expression of dn-cadherin results in the degradation of barrel nets (Fig. 13*C*). Interestingly, the expression of hDNcad after the formation of barrel nets did not disrupt barrel nets (Fig. 13*D*, late 4-OHT), whereas hDNcad expression before the formation of barrel nets effectively disrupted barrel nets (Fig. 13*D*, early 4-OHT). My quantification using confocal microscopic images also supported this conclusion (early 4-OHT, control, n = 3 pups, 41 barrel units; early 4-OHT, hDNcad, n = 3 pups, 52 barrel units; late 4-OHT, control, n = 4 pups, 80 barrel units; late 4-OHT, hDNcad, n = 3 pups, 67 barrel units; from 4 pregnant mice) (Fig. 13*E*). Because it seemed possible that late 4-OHT treatment failed to induce hDNcad, I examined whether hDNcad expression was indeed induced by late 4-OHT treatment by using *in situ* hybridization. I made an *in situ* hybridization probe that detects hDNcad but does not detect endogenous mouse cadherins in the barrel cortex (Fig. 14*A, B*). My late 4-OHT treatment led to strong hDNcad expression, as in the case of early 4-OHT treatment (Fig. 14*B*). Collectively, my results suggest that classic cadherins are required for the formation, rather than the maintenance, of barrel nets.

Discussion

Here, I have shown that classic cadherins are required for the formation, rather than the maintenance, of local circuits in the cerebral cortex during development. Elongation of callosal axons derived from layer 2/3 neurons was not affected by dn-cadherin, suggesting that dn-cadherin selectively inhibited barrel net formation. My results suggest that classic cadherins are also important for the development of presynaptic structures on barrel net axons. My findings uncovered an important role of classic cadherins in local intracortical circuit formation.

Because previous reports showed that multiple classic cadherins are expressed in whisker-related patterns [26,28,31,32,50], I utilized dn-cadherin to suppress these classic cadherins simultaneously and uncovered that classic cadherins are indeed required for barrel net formation. As to how the expression of hDNcad led to disruption of barrel nets, there are four possibilities: (1) reduction in the number of layer 2/3 neurons, (2) inhibition of axonal outgrowth, (3) inhibition of axonal branching and (4) failure of axonal accumulation in septal regions. Since I found the possibilities (1), (2) and (3) to be unlikely, I would conclude that the possibility (4) is a plausible interpretation (Fig. 15).

In order to fully understand the cadherin-mediated mechanisms underlying barrel net formation, there are several important questions to be addressed. First, it would be important to investigate which of the classic cadherins mediate barrel net formation. Combining RNAi and *in utero* electroporation to reveal barrel nets would be appropriate experiments to address this point. Second, because classic cadherins mediate homophilic binding, it seems possible that cadherin molecules on barrel net axons bind to cadherin molecules expressed on other cells in the septa. It would be

intriguing to investigate which neurons in which layers are responsible for this. Alternatively, it seems also possible that cadherins on axons in barrel nets bind to cadherins on neighboring axons in the same barrel net. Third, it would be intriguing to examine how classic cadherins affect the distribution patterns of individual axons during development. When GFP is expressed with conventional *in utero* electroporation, numerous axons in barrel nets are labeled with GFP, and as a result, it is difficult to examine what happens to individual GFP-positive axons, such as branching, elimination, and elongation. Therefore, a combination of PASME (promoter-assisted sparse-neuron multiple-gene labeling using *in utero* electroporation), which is a method for labeling single neurons sparsely [39], with *in vivo* time-lapse two-photon microscopy, or co-culturing layer 2/3 neurons with cadherin-expressing cells [60] would be solutions for probing effects of classic cadherins at the single axon level. Future experiments would be required for obtaining a complete understanding of the mechanisms underlying barrel net formation.

Because of their homophilic binding activity and intriguing expression patterns, classic cadherins have been proposed to be key molecules in the regulation of selective neuronal circuit formation [22,23]. A recent report showed that cadherin-6 mediates axon-target matching of retinal ganglion cell axons in the visual thalamus [61]. Another report demonstrated that cadherin-9 regulates synapse-specific differentiation in the hippocampus [62]. However, involvement of classic cadherins in selective local circuit formation in the neocortex has not been well understood. My results indicate that classic cadherins indeed mediate selective local circuit formation in the neocortex. It remains unclear how cadherins actually regulate selective circuit formation in barrel nets. As discussed earlier, it seems likely that the homophilic binding activity of cadherins is

involved in axon guidance. On the other hand, it seems also possible that cadherins primarily regulate synaptogenesis to stabilize the distribution of axons because previous studies showed that cadherins are important for synaptogenesis [38,62-64]. However, I think that the latter is unlikely for barrel nets because I showed that the density of synapses along individual axons was not affected by expressing dn-cadherin. It would be intriguing to examine the differential roles of cadherins in axon formation and synaptogenesis.

Uncovering the mechanisms underlying the formation of local intracortical circuits would lead to a better understanding of the development and function of the cerebral cortex. Although the anatomical structures and developmental processes of barrel nets have been uncovered [15,16], the function of barrel nets still remains unknown. It seems appropriate to speculate that the function of barrel nets is suppressed in dn-cadherin-expressing animals because of the severe reduction in the number of presynaptic structures by dn-cadherin. Further understanding of the mechanisms underlying barrel net formation would lead to selective loss-of-function experiments involving barrel nets such as the generation of animals without barrel nets, which would reveal their roles in the functioning of the cerebral cortex. Barrel nets seem to be useful for addressing important questions about intracortical local circuits.

Acknowledgments

I express my gratitude to Drs. S. Tsuji, T. Kadowaki and H. Bito (The University of Tokyo) for his continuous support and warm encouragement. I thank Drs. M. Takeichi (RIKEN CDB) and J. Frisén (Karolinska Institutet) for plasmids. I express my gratitude to Drs. T. Sakurai and M. Sato (Kanazawa University) for their technical support. I thank Kawasaki lab members and Z. Blalock for critical discussions and comments on this manuscript, and K. Tanno for technical assistance. I am truly thankful to Drs. T. Toda, L. Iwai and K. Sehara who made tremendous support and encouragement. I am sincerely grateful to Dr. Hiroshi Kawasaki (Kanazawa University) for his caring supervision, continuous encouragement and various kinds of support during the study.

References

1 Petersen, C. C. The functional organization of the barrel cortex. Neuron 56, 339-355 (2007).

2 Huberman, A. D. Mechanisms of eye-specific visual circuit development. Curr Opin Neurobiol 17, 73-80 (2007).

3 Erzurumlu, R. S. & Gaspar, P. Development and critical period plasticity of the barrel cortex. Eur J Neurosci 35, 1540-1553 (2012).

4 Erzurumlu, R. S. & Kind, P. C. Neural activity: sculptor of 'barrels' in the neocortex. Trends Neurosci 24, 589-595 (2001).

5 Fox, K. in Barrel Cortex (ed. Fox, K.) 79-110 (Cambridge University Press, 2008).

6 Lopez-Bendito, G. & Molnar, Z. Thalamocortical development: how are we going to get there? Nat Rev Neurosci 4, 276-289 (2003).

7 O'Leary, D. D., Ruff, N. L. & Dyck, R. H. Development, critical period plasticity, and adult reorganizations of mammalian somatosensory systems. Curr Opin Neurobiol 4, 535-544 (1994).

8 Rebsam, A. & Gaspar, P. in Development and Plasticity in Sensory Thalamus and Cortex (eds. Erzurumlu, R. S., Guido, W. & Molnar, Z.) 183-207 (Springer, 2006).

9 Woolsey, T. A. in Development of Sensory Systems in Mammals (ed. Coleman, J. R.) 461-516 (Wiley, 1990).

10 Toda, T. et al. Birth regulates the initiation of sensory map formation through serotonin signaling. Dev Cell 27, 32-46 (2013).

11 Toda, T. et al. Termination of lesion-induced plasticity in the mouse barrel cortex in the absence of oligodendrocytes. Mol Cell Neurosci 39, 40-49 (2008).

12 Oberlaender, M. et al. Cell type-specific three-dimensional structure of thalamocortical circuits in a column of rat vibrissal cortex. Cereb Cortex 22, 2375-2391 (2012).

13 Meyer, H. S. et al. Cell type-specific thalamic innervation in a column of rat vibrissal cortex. Cereb Cortex 20, 2287-2303 (2010).

14 Meyer, H. S. et al. Number and laminar distribution of neurons in a thalamocortical projection column of rat vibrissal cortex. Cereb Cortex 20, 2277-2286 (2010).

15 Sehara, K., Wakimoto, M., Ako, R. & Kawasaki, H. Distinct developmental principles underlie the formation of ipsilateral and contralateral whisker-related axonal patterns of layer 2/3 neurons in the barrel cortex. Neuroscience 226, 289-304 (2012).

16 Sehara, K. et al. Whisker-related axonal patterns and plasticity of layer 2/3 neurons in the mouse barrel cortex. J Neurosci 30, 3082-3092 (2010).

17 Sehara, K. & Kawasaki, H. Neuronal circuits with whisker-related patterns. Mol Neurobiol 43, 155-162 (2011).

18 Takeichi, M. The cadherin superfamily in neuronal connections and interactions. Nat Rev Neurosci 8, 11-20 (2007).

19 Takeichi, M. Cadherin cell adhesion receptors as a morphogenetic regulator. Science 251, 1451-1455 (1991).

20 Tepass, U., Truong, K., Godt, D., Ikura, M. & Peifer, M. Cadherins in embryonic and neural morphogenesis. Nat Rev Mol Cell Biol 1, 91-100 (2000).

21 Redies, C. & Takeichi, M. Cadherins in the developing central nervous system: an adhesive code for segmental and functional subdivisions. Dev Biol 180, 413-423 (1996).

22 Suzuki, S. C., Inoue, T., Kimura, Y., Tanaka, T. & Takeichi, M. Neuronal circuits are subdivided by differential expression of type-II classic cadherins in postnatal mouse brains. Mol Cell Neurosci 9, 433-447 (1997).

23 Inoue, T., Tanaka, T., Suzuki, S. C. & Takeichi, M. Cadherin-6 in the developing mouse brain: expression along restricted connection systems and synaptic localization suggest a potential role in neuronal circuitry. Dev Dyn 211, 338-351 (1998).

24 Gil, O. D., Needleman, L. & Huntley, G. W. Developmental patterns of cadherin expression and localization in relation to compartmentalized thalamocortical terminations in rat barrel cortex. J Comp Neurol 453, 372-388 (2002).

25 Hertel, N. & Redies, C. Absence of layer-specific cadherin expression profiles in the neocortex of the reeler mutant mouse. Cereb Cortex 21, 1105-1117 (2011).

26 Krishna-K, K., Hertel, N. & Redies, C. Cadherin expression in the somatosensory cortex: evidence for a combinatorial molecular code at the single-cell level. Neuroscience 175, 37-48 (2011).

27 Lefkovics, K., Mayer, M., Bercsenyi, K., Szabo, G. & Lele, Z. Comparative

analysis of type II classic cadherin mRNA distribution patterns in the developing and adult mouse somatosensory cortex and hippocampus suggests significant functional redundancy. J Comp Neurol 520, 1387-1405 (2012).

28 Dye, C. A., El Shawa, H. & Huffman, K. J. A lifespan analysis of intraneocortical connections and gene expression in the mouse II. Cereb Cortex 21, 1331-1350 (2011).

29 Terakawa, Y. W., Inoue, Y. U., Asami, J., Hoshino, M. & Inoue, T. A sharp cadherin-6 gene expression boundary in the developing mouse cortical plate demarcates the future functional areal border. Cereb Cortex 23, 2293-2308 (2013).

30 Inoue, Y. U., Asami, J. & Inoue, T. Cadherin-6 gene regulatory patterns in the postnatal mouse brain. Molecular and Cellular Neuroscience 39, 95-104 (2008).

31 Obst-Pernberg, K., Medina, L. & Redies, C. Expression of R-cadherin and N-cadherin by cell groups and fiber tracts in the developing mouse forebrain: relation to the formation of functional circuits. Neuroscience 106, 505-533 (2001).

32 Huntley, G. W. & Benson, D. L. Neural (N)-cadherin at developing thalamocortical synapses provides an adhesion mechanism for the formation of somatopically organized connections. J Comp Neurol 407, 453-471 (1999).

33 Hirano, S. & Takeichi, M. Cadherins in brain morphogenesis and wiring. Physiol Rev 92, 597-634 (2012).

34 Niwa, H., Yamamura, K. & Miyazaki, J. Efficient selection for high-expression transfectants with a novel eukaryotic vector. Gene 108, 193-199 (1991).

35 Nieman, M. T., Kim, J. B., Johnson, K. R. & Wheelock, M. J. Mechanism of extracellular domain-deleted dominant negative cadherins. J Cell Sci 112 (Pt 10), 1621-1632 (1999).

36 Barnabe-Heider, F. et al. Genetic manipulation of adult mouse neurogenic niches by in vivo electroporation. Nat Methods 5, 189-196 (2008).

37 Fujimori, T. & Takeichi, M. Disruption of epithelial cell-cell adhesion by exogenous expression of a mutated nonfunctional N-cadherin. Mol Biol Cell 4, 37-47 (1993).

38 Togashi, H. et al. Cadherin regulates dendritic spine morphogenesis. Neuron 35, 77-89 (2002).

39 Ako, R. et al. Simultaneous visualization of multiple neuronal properties with single-cell resolution in the living rodent brain. Mol Cell Neurosci 48, 246-257 (2011).

40 Kawasaki, H., Iwai, L. & Tanno, K. Rapid and efficient genetic manipulation of gyrencephalic carnivores using in utero electroporation. Mol Brain 5, 24 (2012).

41 Kawasaki, H., Toda, T. & Tanno, K. In vivo genetic manipulation of cortical progenitors in gyrencephalic carnivores using in utero electroporation. Biol Open 2, 95-100 (2013).

42 Yamasaki, T. et al. Stress-activated protein kinase MKK7 regulates axon elongation in the developing cerebral cortex. J Neurosci 31, 16872-16883 (2011).

43 Hayakawa, I. & Kawasaki, H. Rearrangement of retinogeniculate projection patterns after eye-specific segregation in mice. PLoS One 5, e11001 (2010).

44 Iwai, L. et al. FoxP2 is a parvocellular-specific transcription factor in the visual thalamus of monkeys and ferrets. Cereb Cortex 23, 2204-2212 (2013).

45 Kawasaki, H., Crowley, J. C., Livesey, F. J. & Katz, L. C. Molecular organization of the ferret visual thalamus. J Neurosci 24, 9962-9970 (2004).

46 Iwai, L. & Kawasaki, H. Molecular development of the lateral geniculate nucleus in the absence of retinal waves during the time of retinal axon eye-specific segregation. Neuroscience 159, 1326-1337 (2009).

47 Meijering, E. et al. Design and validation of a tool for neurite tracing and analysis in fluorescence microscopy images. Cytometry A 58, 167-176 (2004).

48 Meijering, E. Neuron tracing in perspective. Cytometry A 77, 693-704 (2010).

49 R: A language and environment for statistical computing. v. 3.1.0 (R Foundation for Statistical Computing, Vienna, Austria, 2014).

50 Huntley, G. W. Dynamic aspects of cadherin-mediated adhesion in synapse development and plasticity. Biol Cell 94, 335-344 (2002).

51 Kawauchi, T. et al. Rab GTPases-dependent endocytic pathways regulate neuronal migration and maturation through N-cadherin trafficking. Neuron 67, 588-602 (2010).

52 Matsuda, T. & Cepko, C. L. Controlled expression of transgenes introduced by in vivo electroporation. Proc Natl Acad Sci USA 104, 1027-1032 (2007).

53 Fremeau, R. T., Jr. et al. The expression of vesicular glutamate transporters defines two classes of excitatory synapse. Neuron 31, 247-260 (2001).

54 Fujiyama, F., Furuta, T. & Kaneko, T. Immunocytochemical localization of candidates for vesicular glutamate transporters in the rat cerebral cortex. J Comp Neurol 435, 379-387 (2001).

55 Riehl, R. et al. Cadherin function is required for axon outgrowth in retinal ganglion cells in vivo. Neuron 17, 837-848 (1996).

56 Hevner, R. F. et al. Beyond laminar fate: toward a molecular classification of cortical projection/pyramidal neurons. Dev Neurosci 25, 139-151 (2003).

57 Arlotta, P. et al. Neuronal subtype-specific genes that control corticospinal motor neuron development in vivo. Neuron 45, 207-221 (2005).

58 Nakagawa, Y. & O'Leary, D. D. Dynamic patterned expression of orphan nuclear receptor genes RORalpha and RORbeta in developing mouse forebrain. Dev Neurosci 25, 234-244 (2003).

59 Schaeren-Wiemers, N., Andre, E., Kapfhammer, J. P. & Becker-Andre, M. The expression pattern of the orphan nuclear receptor RORbeta in the developing and adult rat nervous system suggests a role in the processing of sensory information and in circadian rhythm. Eur J Neurosci 9, 2687-2701 (1997).

60 Walter, J., Kern-Veits, B., Huf, J., Stolze, B. & Bonhoeffer, F. Recognition of position-specific properties of tectal cell membranes by retinal axons in vitro. Development 101, 685-696 (1987).

61 Osterhout, J. A. et al. Cadherin-6 mediates axon-target matching in a non-image-forming visual circuit. Neuron 71, 632-639 (2011).

62 Williams, M. E. et al. Cadherin-9 regulates synapse-specific differentiation in the developing hippocampus. Neuron 71, 640-655 (2011).

63 Bozdagi, O., Valcin, M., Poskanzer, K., Tanaka, H. & Benson, D. L. Temporally distinct demands for classic cadherins in synapse formation and maturation. Mol Cell Neurosci 27, 509-521 (2004).

64 Inoue, A. & Sanes, J. R. Lamina-specific connectivity in the brain: regulation by N-cadherin, neurotrophins, and glycoconjugates. Science 276, 1428-1431 (1997).

Figures

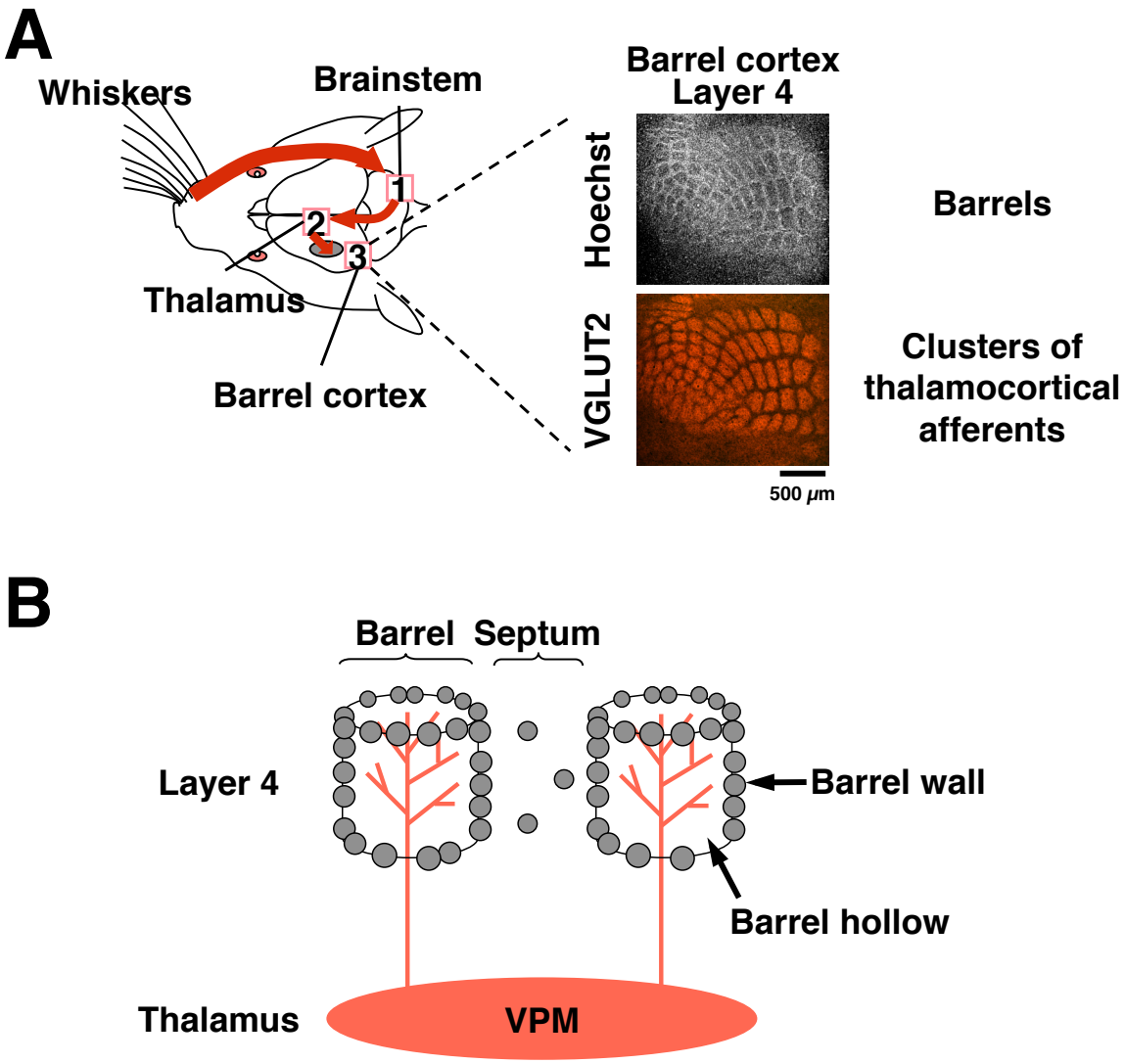

Figure 1. Schematic representation of the somatosensory pathway in mice
(A) Pathways from whiskers to barrels. (Left) Somatosensory stimuli from the whiskers are transmitted through the brainstem and the contralateral thalamus before reaching the primary somatosensory cortex (barrel cortex). (Right) The whisker-related pattern of barrels in layer 4 of barrel cortex is visualized by Hoechst staining. Thalamocortical axons from VPM of thalamus are revealed by VGLUT2 immunostaining. The spatial pattern of barrels represents that of whiskers on the contralateral snout, with each barrel having a one-to-one relationship with the corresponding whisker. *(B)* The schema of the somatosensory pathway from the thalamus to the barrel cortex. Thalamocortical afferents from the VPM thalamic nucleus form axonal clusters in the barrel hollows (the center of each barrel). Layer 4 neurons (indicated by gray circles) surround these axonal clusters, forming barrel walls. The cell-sparse region in layer 4 between barrels is called the septum.

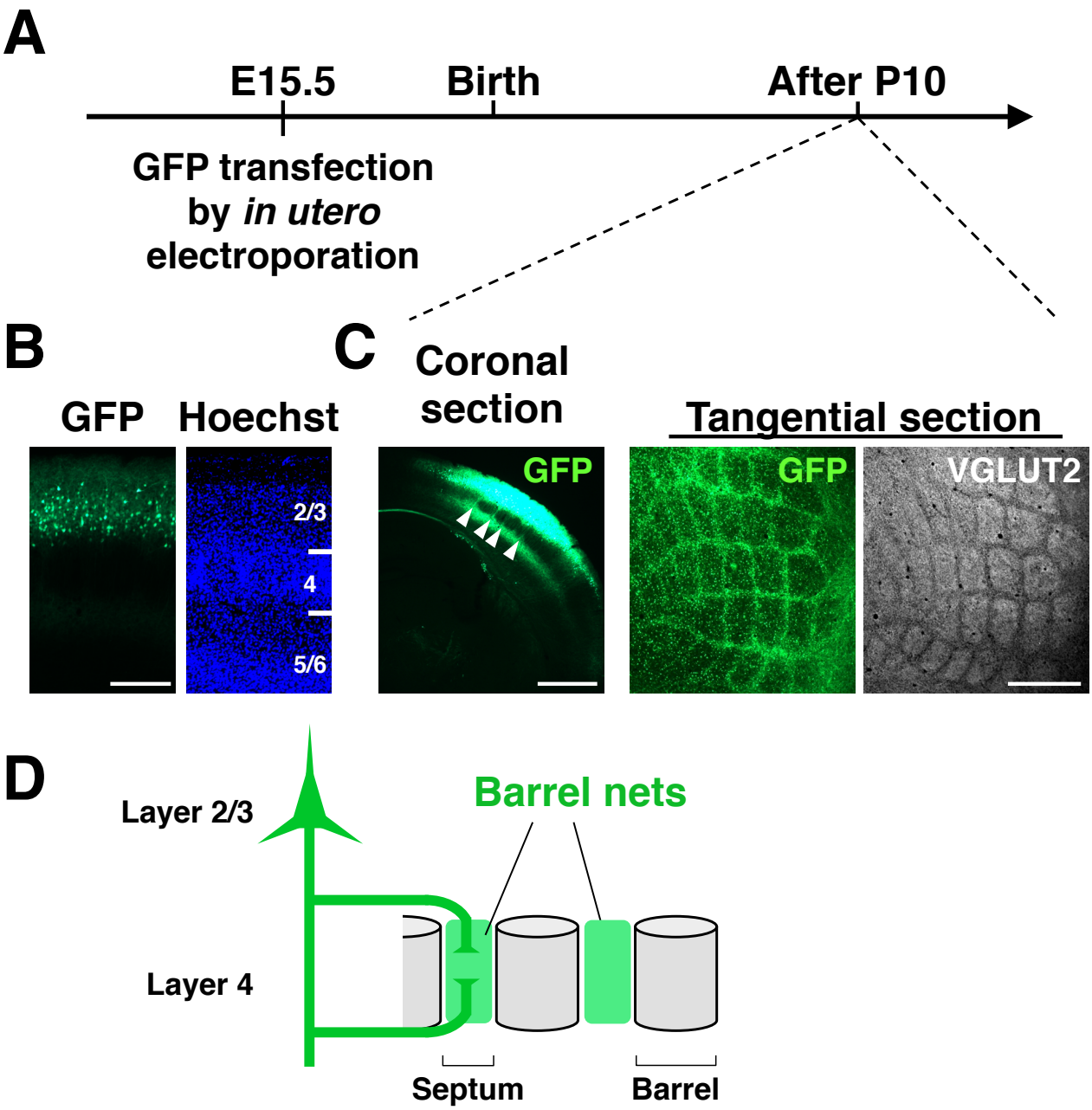

Figure 2. "Barrel nets" is axonal trajectories of layer 2/3 neurons and is preferentially distributed in septal regions in layer 4

(*A*) Experimental procedure for labeling axons of layer 2/3 neurons with GFP using *in utero* electroporation. The electroporation was performed at E15.5. Pups were developed normally and their brains were collected postnatally. (*B*) Location of GFP-positive neurons in the barrel cortex. GFP positive cells were expressed selectively in layer 2/3 when *in utero* electroporation was performed at E15.5. The brightness of GFP images was adjusted to visualize the somata. Scale bar = 250 µm. (*C*) Visualization of barrel nets after P10. (Left) GFP fluorescence in coronal sections prepared at P15. The brightness of GFP images was adjusted to visualize the axons of layer 2/3 neurons. Note that GFP-positive axons from layer 2/3 neurons are accumulated in septal region indicated by arrowheads in layer 4. Scale bar = 1 mm. (Middle and right) Tangential section prepared at P23 were immunostained with anti-VGLUT2 antibody. Note that GFP-positive axons show a pattern complementary to VGLUT2-positive thalamocortical axonal patches. Scale bar = 500 µm. (*D*) A diagram for the composition of barrel nets. Axons from layer 2/3 neuron are distributed preferentially in the septal region of layer 4 in the barrel cortex.

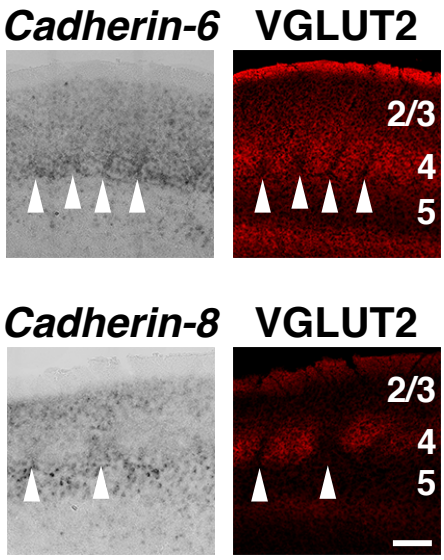

Figure 3. Expression of cadherins in the developing barrel cortex
Coronal sections of the mouse barrel cortex were prepared at P10 (for the *cadherin-8* probe) or P15 (for the *cadherin-6* probe). After *in situ* hybridization (left), immunostaining with anti-VGLUT2 antibody (right) were performed. The ages were chosen so that the staining reveals obvious whisker-related patterns. Note that *cadherin-6* and *cadherin-8* were preferentially expressed in septal regions (arrowheads) in layer 4, as well as in layer 2/3. Scale bar = 200 μm.

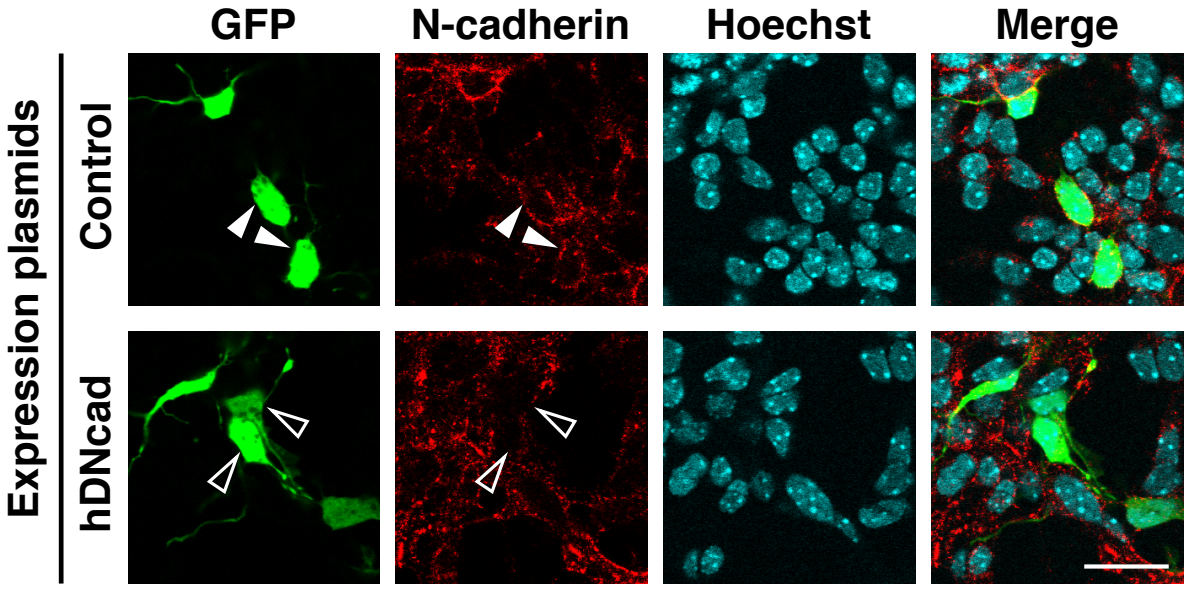

Figure 4. The effect of dn-cadherin on endogenous cadherin expression in layer 2/3 neurons

hDNcad and GFP (as a transfection marker) were co-expressed in layer 2/3 neurons using *in utero* electroporation at E15.5, and dissociated primary cultures were prepared from the transfected cerebral cortex the day after. Neurons at DIV2 were stained using antibody raised against the extracellular domain of N-cadherin without permeabilization to detect cell surface expression of N-cadherin. Confocal microscopic images showed that N-cadherin immunoreactivity was found at the cell surface of layer 2/3 neurons in control conditions as expected (upper panels, filled arrowheads), whereas it was markedly suppressed in hDNcad-expressing neurons (lower panels, open arrowheads), suggesting that the function of cadherins is suppressed by hDNcad in layer 2/3 neurons. Scale bar = 20 μm.

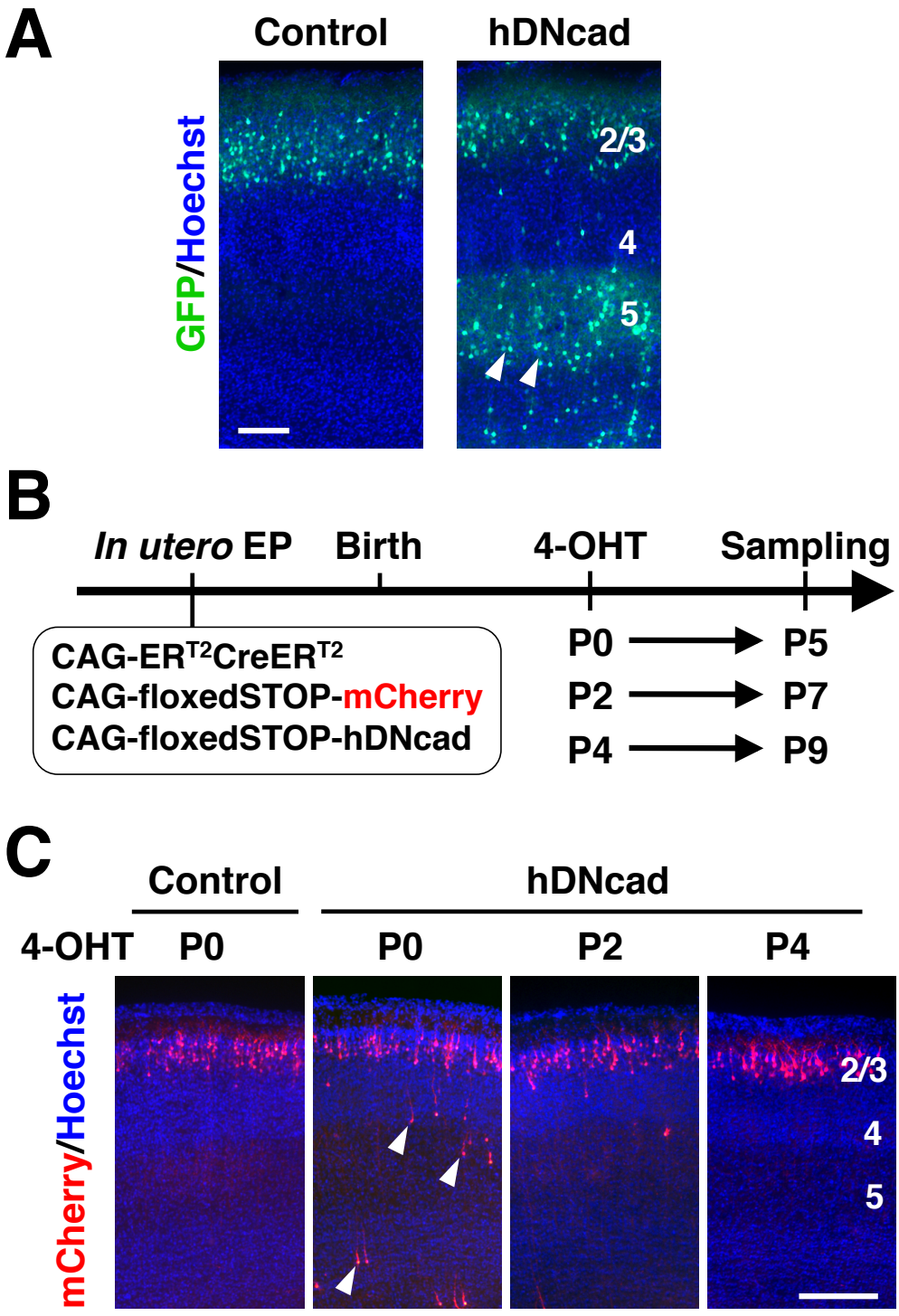

Figure 5. The effect of dn-cadherin on migration of transfected layer 2/3 neurons
(*A*) Layer 2/3 neurons were transfected with pCAG-GFP plus either pCAG vector (control) or pCAG-hDNcad (hDNcad) using *in utero* electroporation at E15.5. Coronal sections were prepared at P16 and stained with Hoechst 33342. Note that migration of GFP-positive transfected layer 2/3 neurons was severely impaired by hDNcad expression (arrowheads). Cortical layers are indicated with numbers. Scale bar = 150 μm. (*B*) Experimental procedure for temporal regulation of dn-cadherin expression. After layer 2/3 neurons were transfected with the indicated plasmids using *in utero* electroporation, pups were treated with 4-OHT at the indicated time points during development. Coronal sections were prepared 5 days later and stained with Hoechst 33342. (*C*) Migration was impaired by 4-OHT treatment at P0 (arrowheads), but not by the treatment at P2 or P4 in hDNcad sample. The experiments were performed as described in Figure 5*B*. Cortical layers are indicated with numbers. Scale bar = 250 μm.

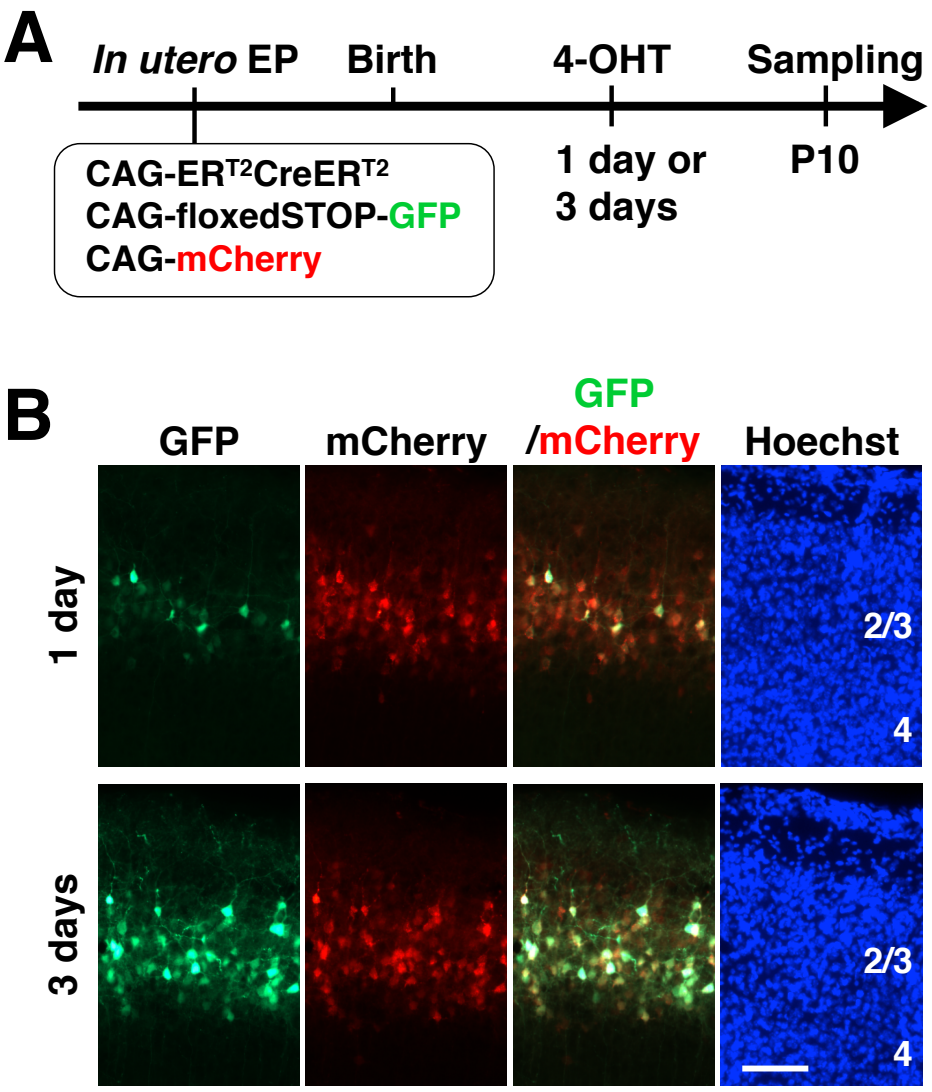

Figure 6. Efficient gene expression was achieved by multiple 4-OHT treatments (*A*) Experimental procedure. After layer 2/3 neurons were co-transfected with *in utero* electroporation at E15.5, pups were treated with 4-OHT once or 3 times daily. Coronal sections were prepared at P10 and stained with Hoechst 33342. (*B*) 4-OHT treatment for 3 consecutive days gave higher recombination efficiency. Note that transfection efficiency was indistinguishable between 1-day and 3-day treatment as revealed with mCherry signals, whereas GFP signals were markedly enhanced by 3-day treatment. Cortical layers are indicated with numbers. Scale bar = 100 μm.

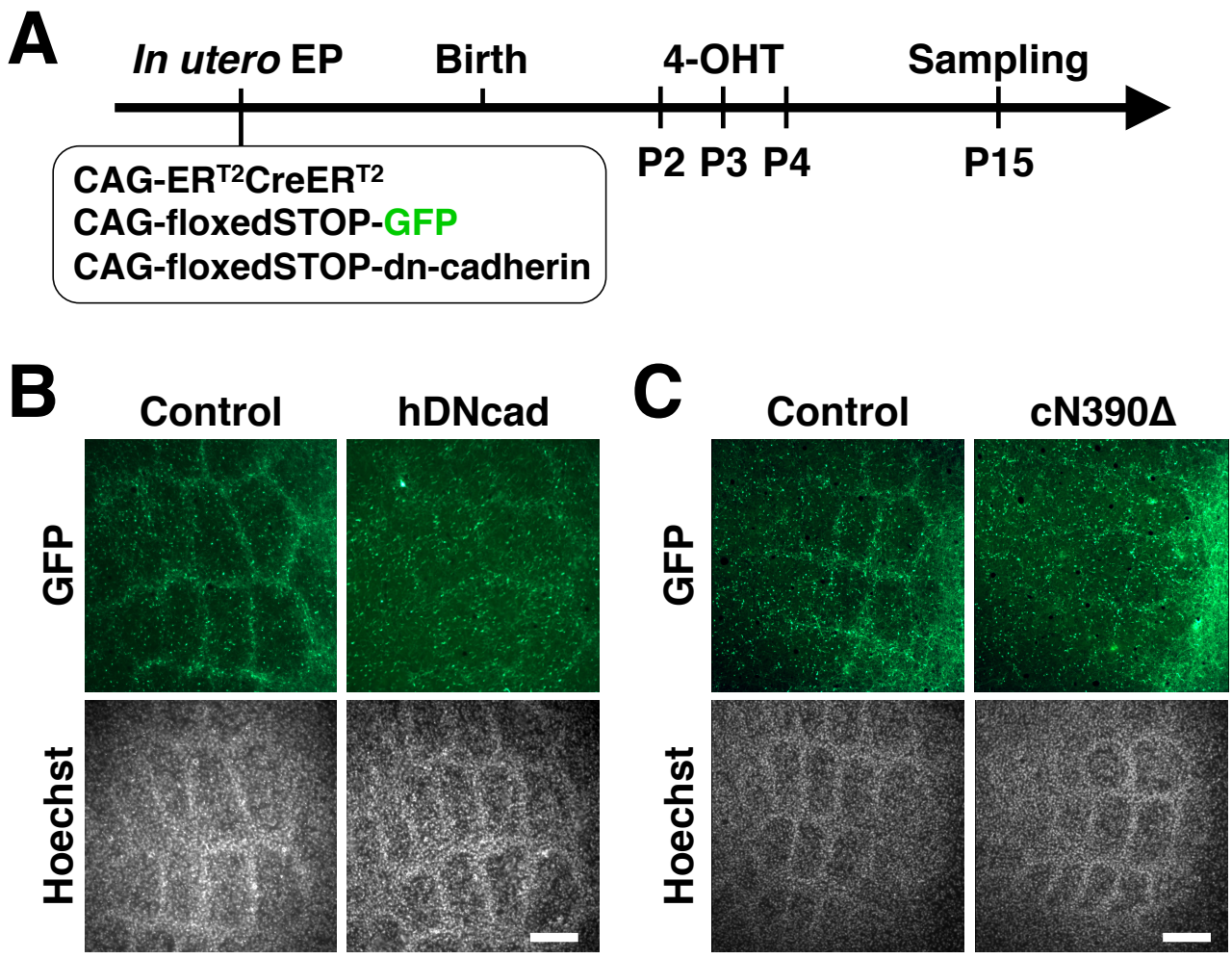

Figure 7. The effects of dn-cadherin expression on barrel net patterns in tangential sections

(*A*) Experimental procedure. After layer 2/3 neurons were transfected with the indicated plasmids using *in utero* electroporation at E15.5, pups were treated with 4-OHT 3 times at the indicated time points. Tangential sections were prepared at P15, and sections containing layer 4 were stained with Hoechst 33342. (*B*) Expression of hDNcad in layer 2/3 neurons strongly inhibited barrel net formation (hDNcad), whereas control plasmid did not affect barrel net patterns (control). (*C*) Expression of cN390Δ, another dn-cadherin construct, gave consistent results. Note that the pattern of cytoarchitectonic barrels revealed with Hoechst staining was not apparently affected by dn-cadherin expression (lower panels). Scale bars = 200 μm.

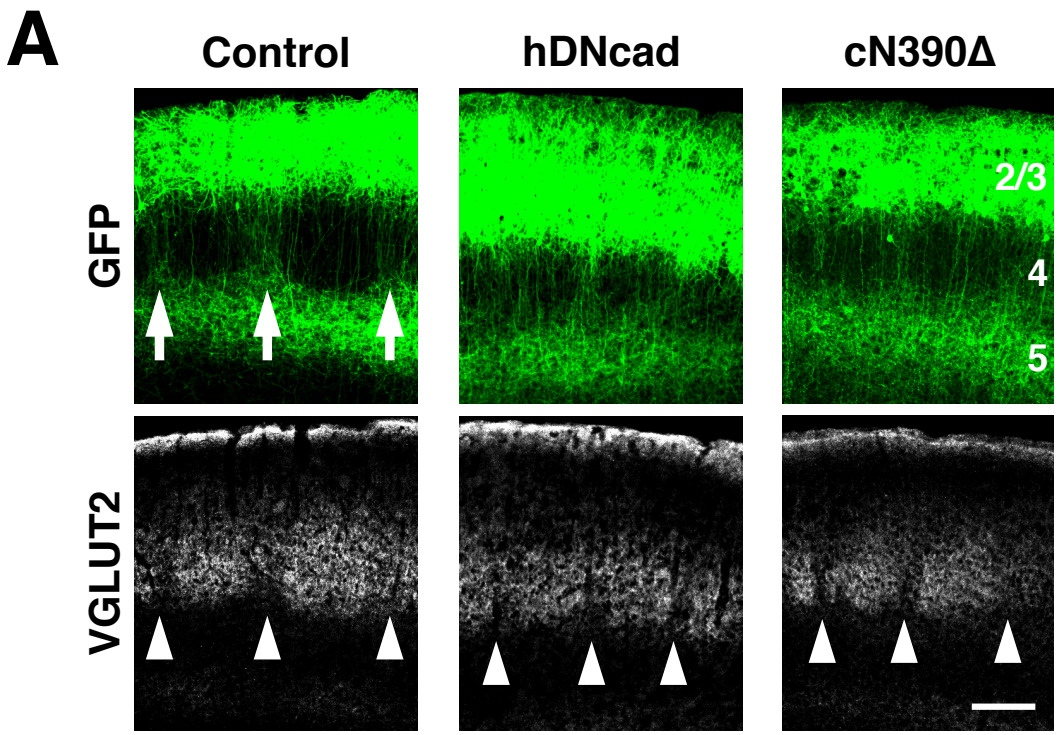

Figure 8. The effects of dn-cadherin expression on barrel net patterns in coronal sections

(*A*) *In utero* electroporation and 4-OHT treatment were performed as described in Figure 7*A*. Coronal sections were prepared at P15 and stained with anti-VGLUT2 antibody, which visualizes whisker-related patterns of thalamocortical axon (TCA) patches. Confocal microscopic images are shown. Although GFP-positive axons are predominantly accumulated in septal regions of control samples (arrows), such accumulation was severely impaired in dn-cadherin samples (hDNcad and cN390Δ). Note that TCA patches revealed with VGLUT2 antibody were not apparently affected by dn-cadherin. Arrowheads indicate septal regions revealed with VGLUT2 staining. Cortical layers are indicated with numbers. Scale bar = 50 μm.

(to be continued)

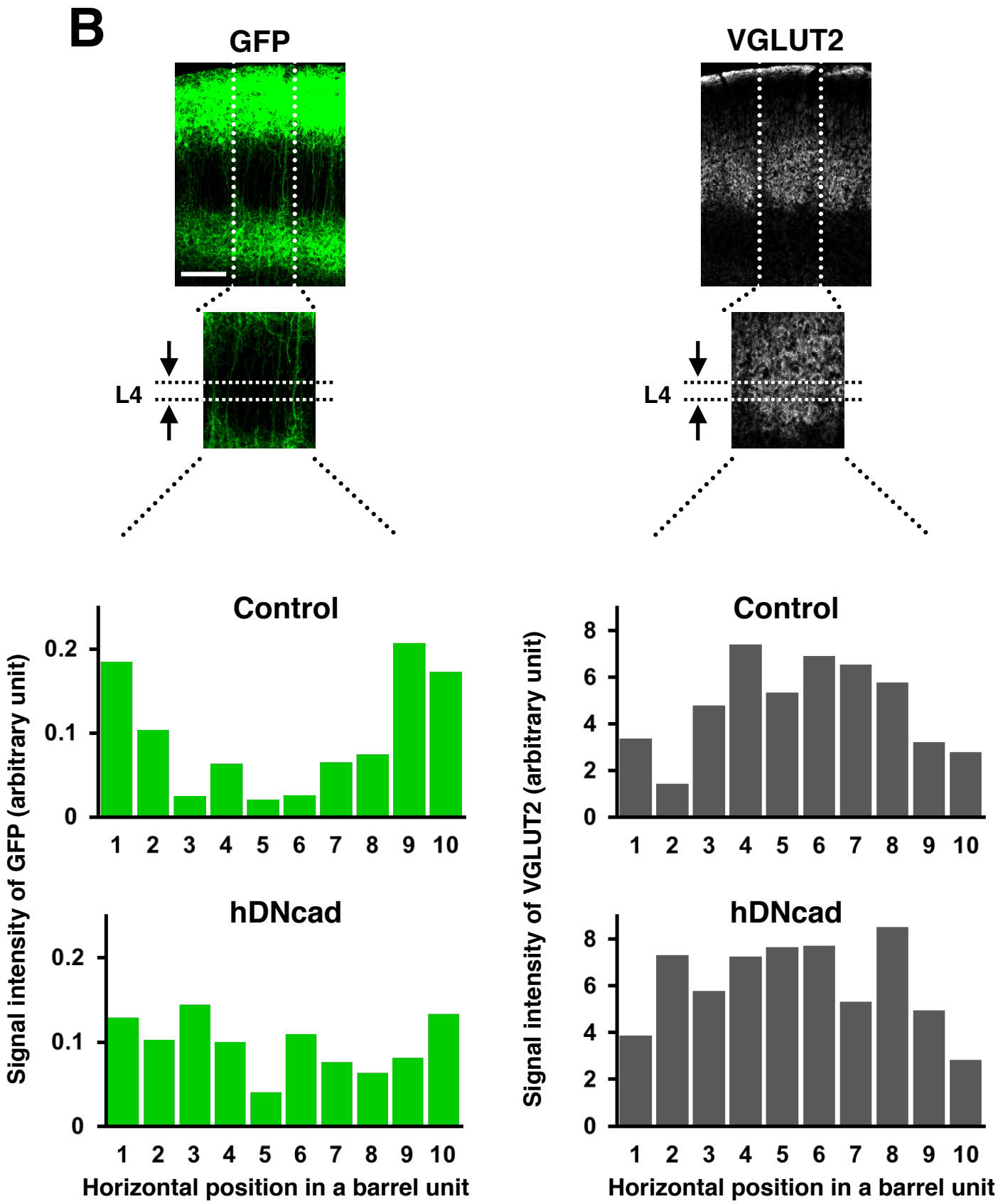

(Figure 8. continued)

(*B*) Quantification of the distribution patterns of GFP signals and VGLUT2 signals within barrel units. Signal intensities in layer 4 within single barrel units were measured and summed along the horizontal x-axis. Each barrel unit was divided into ten barrel subunits of equal width (numbers under each histogram indicate the positions of individual barrel subunits), and the measured values were summed within individual barrel subunits. The averaged values of each barrel subunit were plotted against the horizontal position of the subunit within a barrel unit. See Materials and Methods for details. Scale bar = 50 μm.

(to be continued)

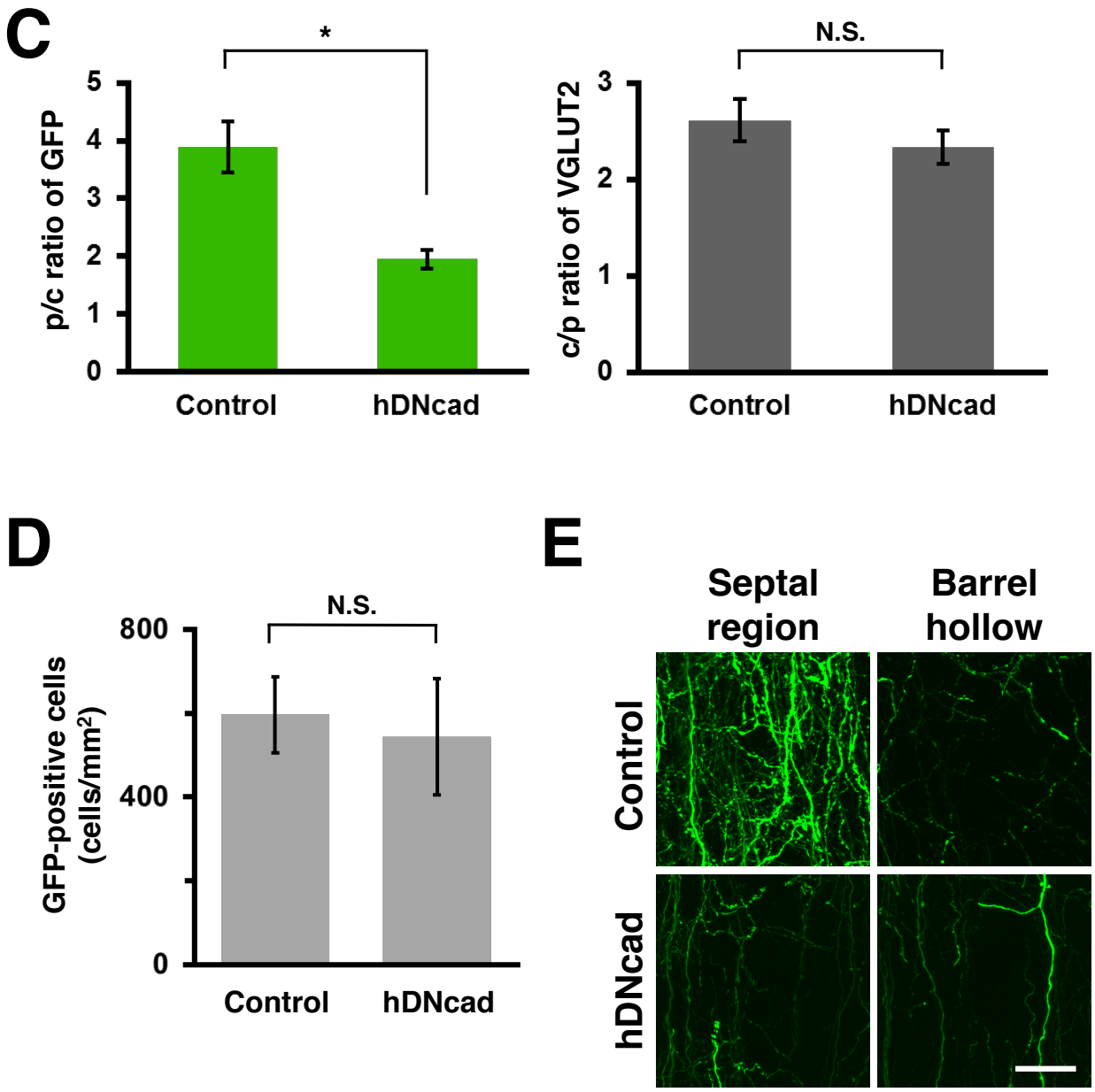

(Figure 8. continued)
(*C*) Quantitative analyses of the effects of dn-cadherin on barrel net formation (see Materials and Methods for detailed procedures). The p/c ratio of GFP signals was significantly lower in hDNcad samples, whereas the c/p ratio of VGLUT2 was not. **P* < 0.05, N.S. *P* > 0.3, Welch's *t*-test. Error bars indicate the standard error of the mean (SEM). n = 3 pups for control, 3 pups for hDNcad. (*D*) Quantitative analysis of the numbers of GFP-positive neurons in layer 2/3. Coronal sections of 50 μm thickness were examined using a confocal microscope, and the densities of GFP-positive cells were examined. No significant difference was detected between control and hDNcad samples (N.S. *P* > 0.5, Mann-Whitney's *U*-test; n = 3 pups for control, 3 pups for hDNcad). Error bars indicate SEM. (*E*) High-magnification confocal microscopic analysis of GFP-positive axons in septal regions and barrel hollows. GFP-positive fine axons in septal regions were much fewer in hDNcad samples than in control samples. Scale bar = 20 μm.

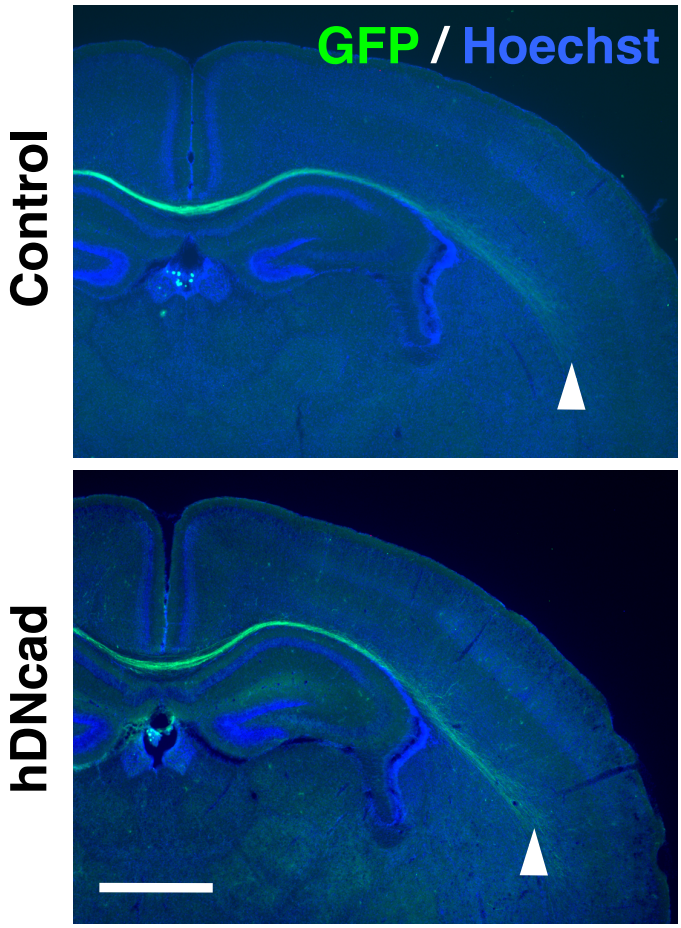

Figure 9. The effect of dn-cadherin expression on callosal axons derived from layer 2/3 neurons
In utero electroporation and 4-OHT treatment were performed as described in Figure 7*A*. Coronal sections were prepared at P15, and were stained with Hoechst 33342. The cortex contralateral to the transfected side is shown, and therefore GFP-positive axons are callosal axons derived from layer 2/3 neurons of transfected side (not shown). The extension of GFP-positive callosal axons was not suppressed by hDNcad expression (arrowheads). Scale bar = 1 mm.

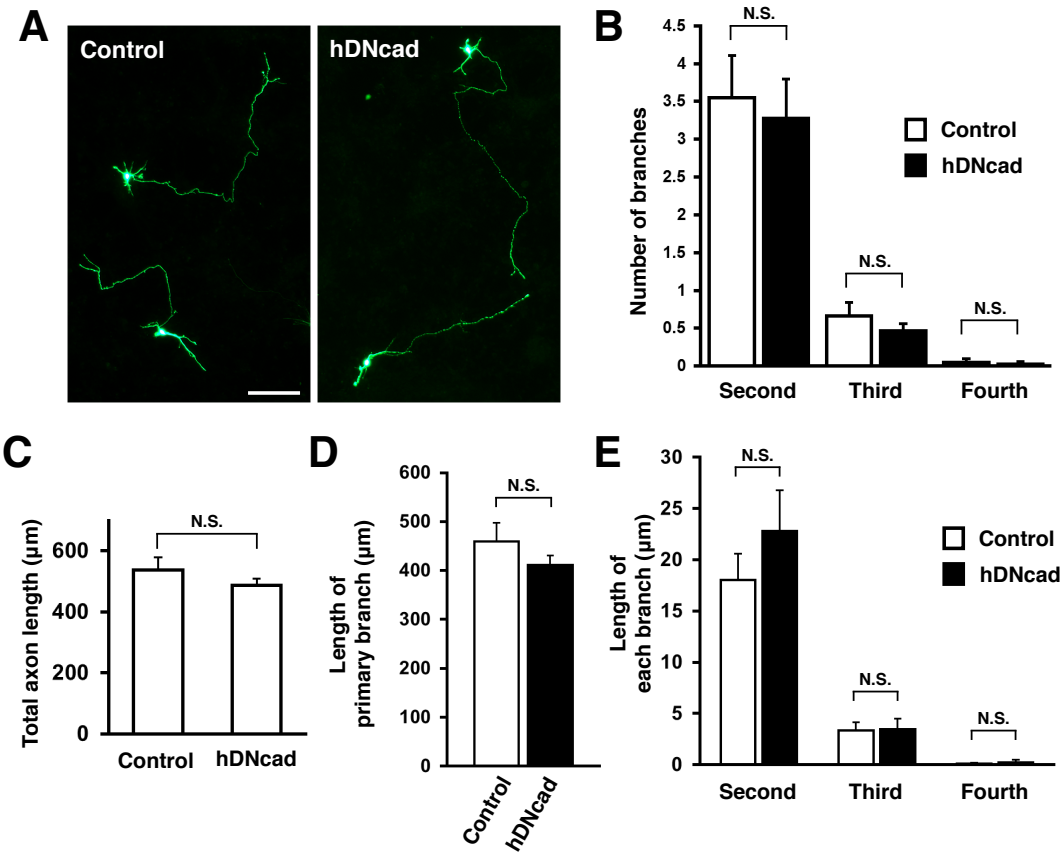

Figure 10. The effects of dn-cadherin on the morphology of layer 2/3 neurons *in vitro*

(*A*) Representative images of primary cultured layer 2/3 neurons electroporated with GFP expression plasmids plus either control (left) or hDNcad expression (right) plasmids at E15.5. Note that their morphologies were indistinguishable from each other. Scale bar = 100 μm. (*B*-*E*) Quantification of morphologies of the transfected neurons. No significant differences were observed in the number of branches (*B*), total axon length (*C*), the length of the primary axon branch (*D*), and the length of higher-order axon branches (*E*). N.S. $P > 0.1$, Welch's *t*-test; n = 7 for each sample. Error bars in all graphs indicate SEM.

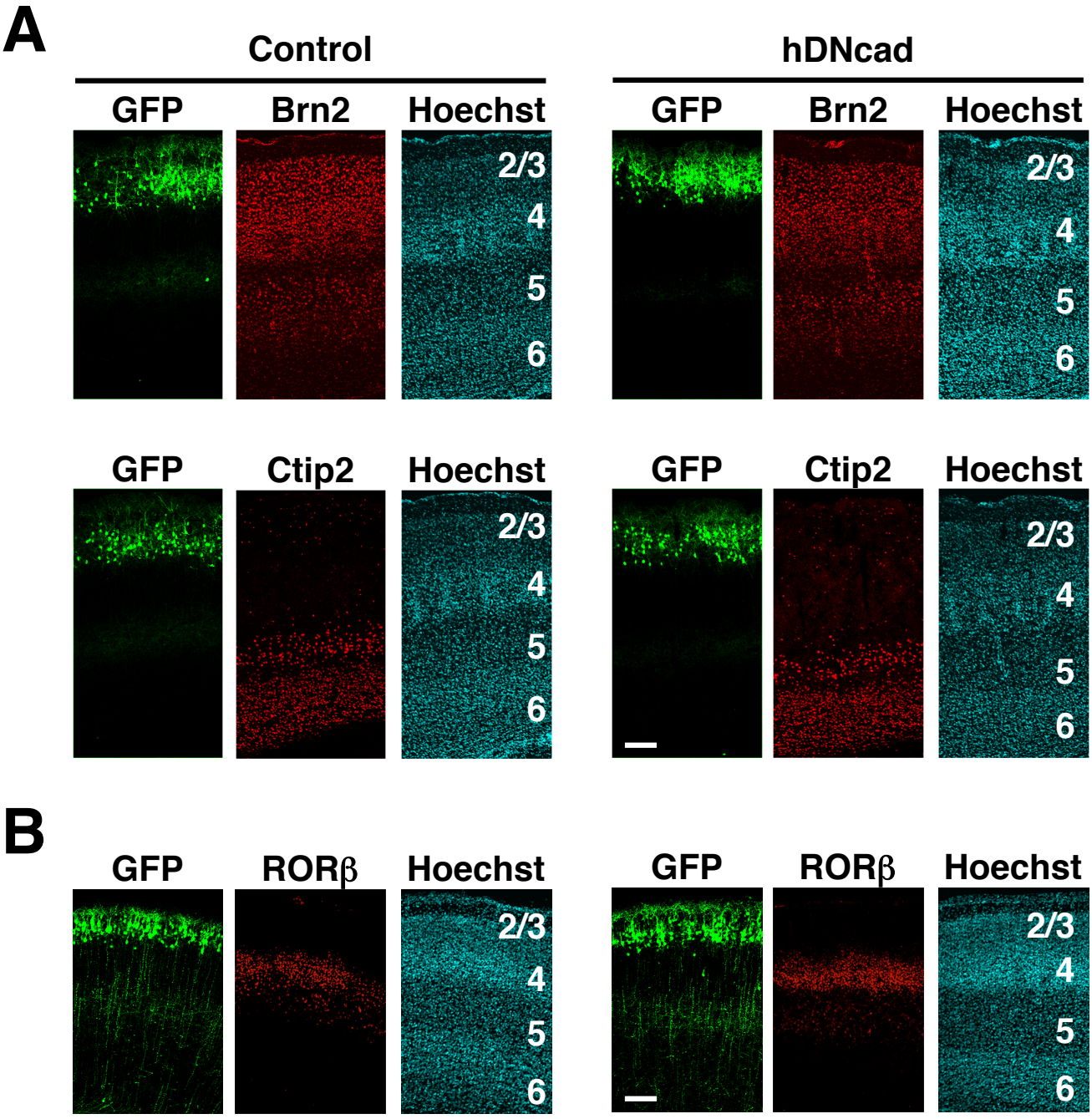

Figure 11. The expression patterns of layer markers in the hDNcad-transfected cortex

In utero electroporation and 4-OHT treatment were performed as described in Figure 7*A*. Coronal sections were stained with anti-Brn2, anti-RORβ and anti-Ctip2 antibodies. (*A*, *B*) Confocal microscopic images of Brn2 and Ctip2 at P15 (*A*) and of RORβ at P5 (*B*). The expression of layer markers was not affected in GFP-positive hDNcad-transfected neurons. Cortical layers are indicated with numbers. Scale bars = 150 μm.

(to be continued)

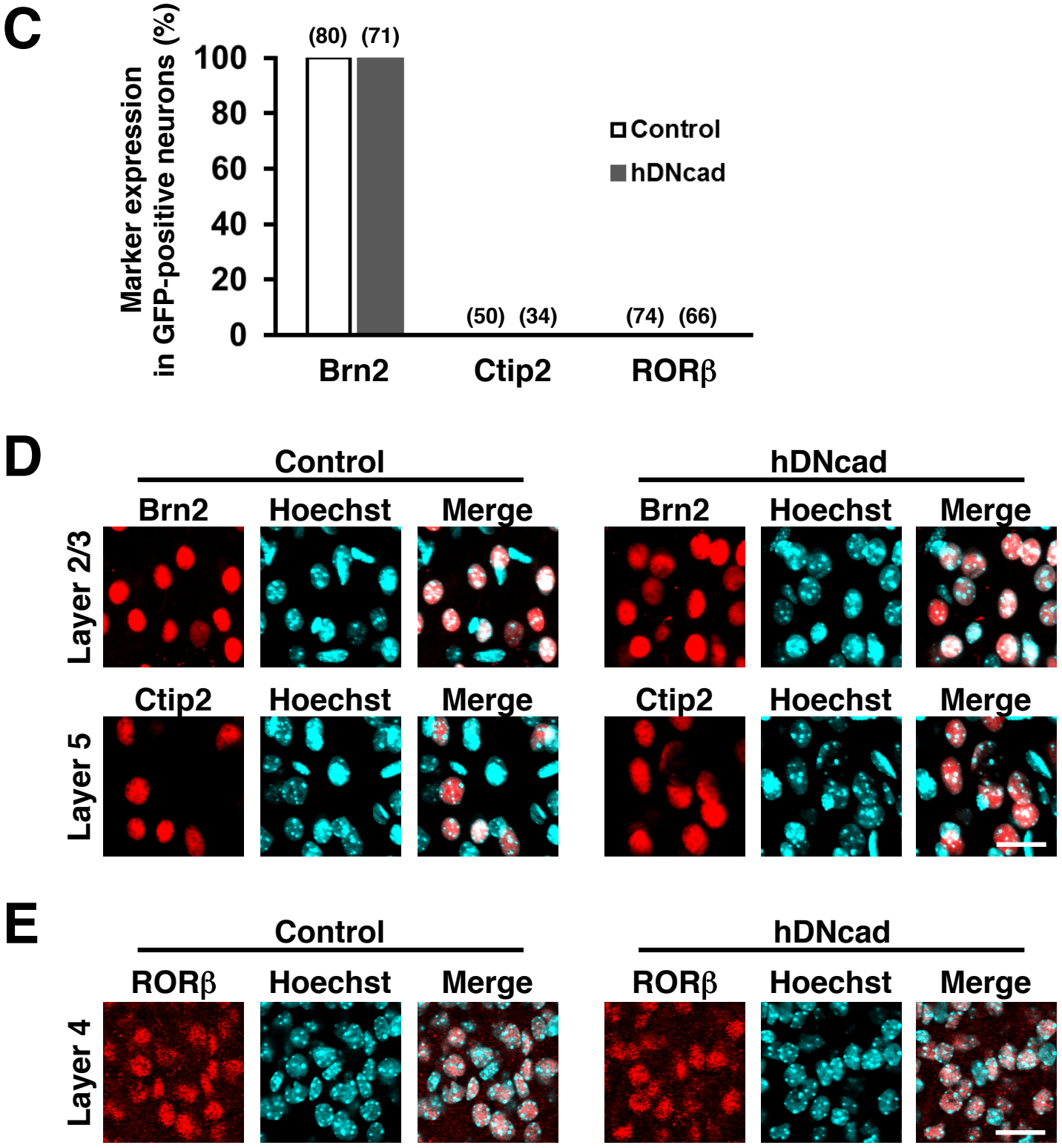

(Figure 11. continued)
(*C*) Quantification of marker expression. The numbers of GFP-positive cells examined are indicated in parenthesis. (*D*, *E*) High-magnification confocal microscopic images at P15 (*D*) and P5 (*E*). Brn2, Ctip2, and RORβ signals were localized in Hoechst-positive nuclei. Scale bars = 20 *μ*m.

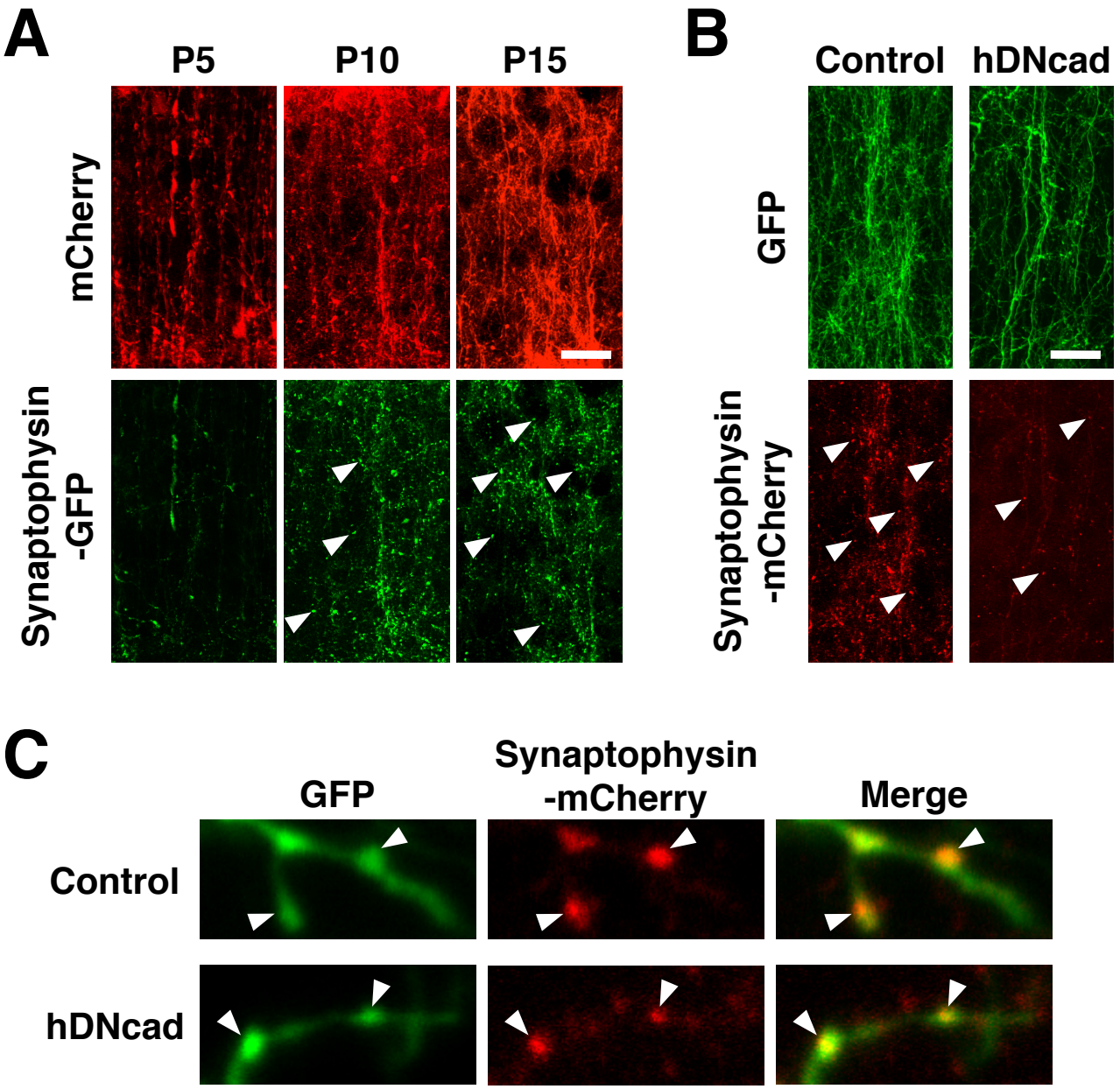

Figure 12. The effect of hDNcad on presynaptic structures on barrel nets
(*A*) Developmental time course of the formation of presynaptic structures. Layer 2/3 neurons were transfected with pCAG-mCherry and pCAG-synaptophysin-GFP at E15.5, and coronal sections were prepared at the indicated ages. Septal regions in layer 4 are shown. mCherry-positive axons of layer 2/3 neurons in barrel nets increased from P5 to P15. Accordingly, GFP-positive puncta also markedly increased (arrowheads). Scale bar = 25 μm. (*B*) The effect of hDNcad on presynaptic structures on barrel nets. Layer 2/3 neurons were transfected with pCAG-synaptophysin-mCherry, pCAG-ER^{T2}CreER^{T2}, pCAG-floxedSTOP-GFP plus either pCAG-floxedSTOP-hDNcad or pCAG-floxedSTOP control vector at E15.5, and pups were treated with 4-OHT 3 times. Coronal sections were prepared at P15. Septal regions in layer 4 are shown. The expression of hDNcad resulted in the reduction of mCherry-positive puncta (arrowheads). Scale bar = 25 μm. (*C*) High magnification images of mCherry-positive puncta (red, arrowheads) and GFP-positive axon branches (green). Scale bar = 1 μm.

(to be continued)

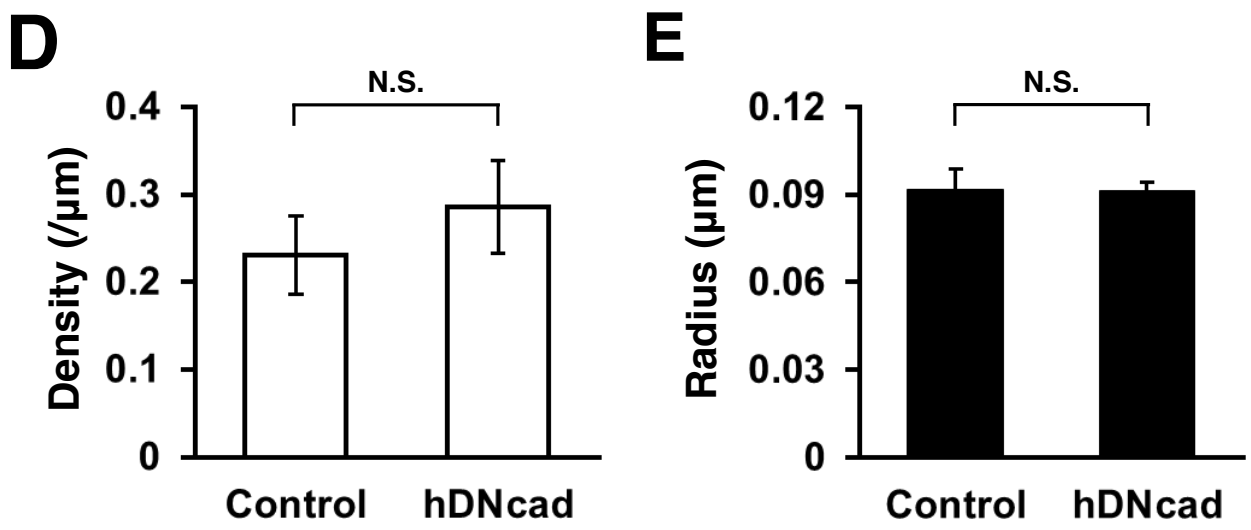

(Figure 12. continued)
(*D*) The density of mCherry-positive puncta along GFP-positive axons in hDNcad samples was not significantly different from that in control samples. N.S. $P > 0.2$, Mann-Whitney's *U*-test; n = 3 pups for both conditions. Error bars indicate SEM. (*E*) The size of individual mCherry-positive puncta in hDNcad samples was not significantly different from that in control samples. N.S. $P > 0.2$, Mann-Whitney's *U*-test; n = 3 pups for both conditions. Error bars indicate SEM.

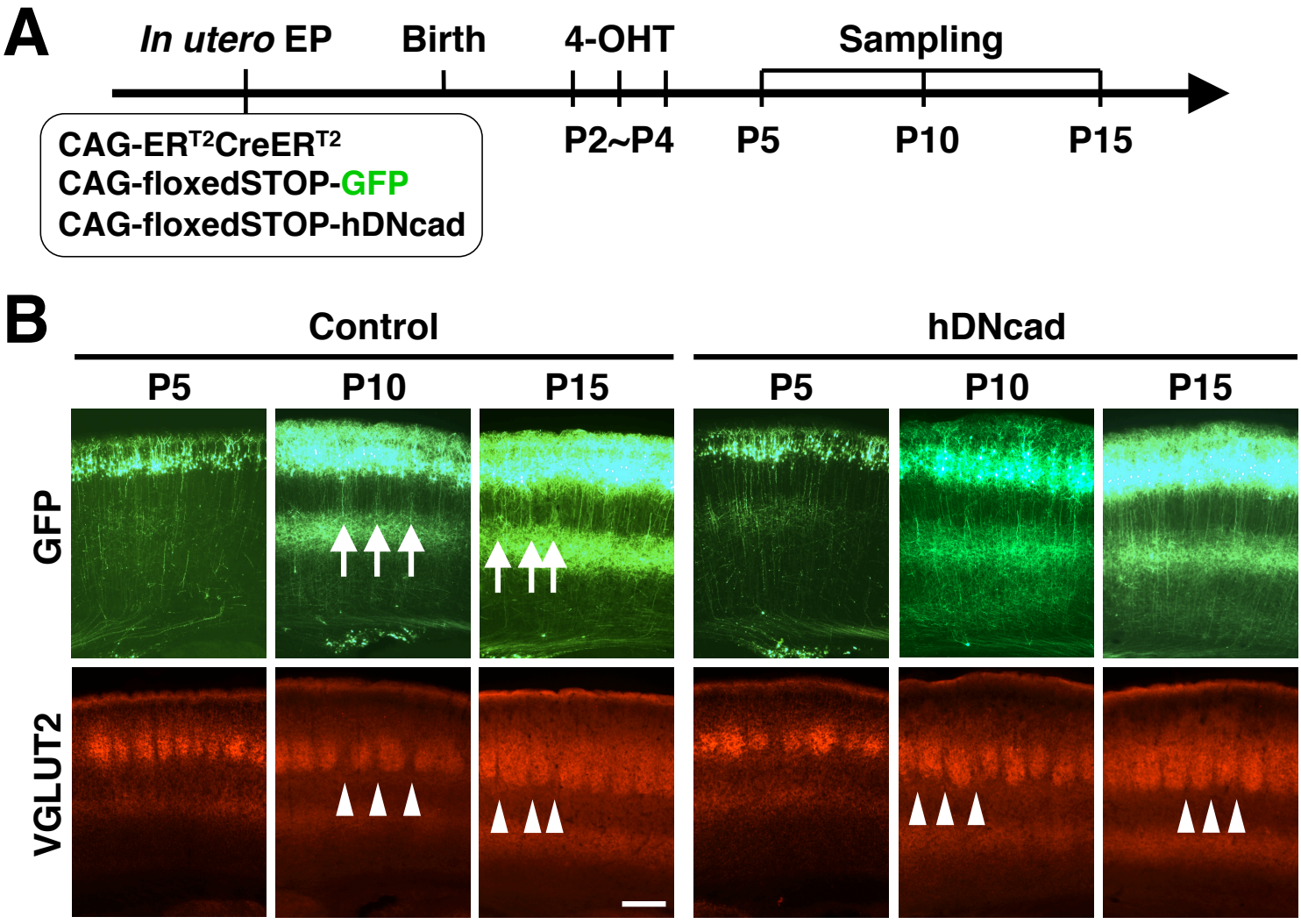

Figure 13. Cadherin is required for the formation, rather than the maintenance, of barrel nets

(*A*) Experimental procedure for examining time course of barrel net formation. *In utero* electroporation and 4-OHT treatment were performed as described, and coronal sections were prepared at the indicated time points. (*B*) Barrel nets were not visible at any ages examined in hDNcad samples, whereas the pattern of barrel nets was visible after P10 in control samples (arrows). Arrowheads indicate septal regions. Scale bar = 250 μm. (*C*) Experimental procedures for early and late 4-OHT treatments. *In utero* electroporation was performed as described in Figure 14*A*, and 4-OHT treatment was performed at P2-P4 (early 4-OHT) or P15-P17 (late 4-OHT). Coronal sections were prepared about two weeks later, and stained with Hoechst 33342. (*D*) The effects of early and late 4-OHT treatments on barrel net patterns. Note that barrel net patterns were strongly disrupted by early 4-OHT treatment, whereas they were not affected by late 4-OHT treatment (arrows). Arrowheads indicate the septal region. Scale bar = 200 μm. (*E*) Quantification of the p/c ratio. Early 4-OHT treatment significantly reduced the p/c ratio in hDNcad-transfected samples, whereas late 4-OHT treatment did not. $^*P < 0.05$, N.S. $P > 0.2$, Welch's *t*-test (early 4-OHT, control, n = 3 pups; early 4-OHT, hDNcad, n = 3 pups; late 4-OHT, control, n = 4 pups; late 4-OHT, hDNcad, n = 3 pups). Error bars indicate SEM.

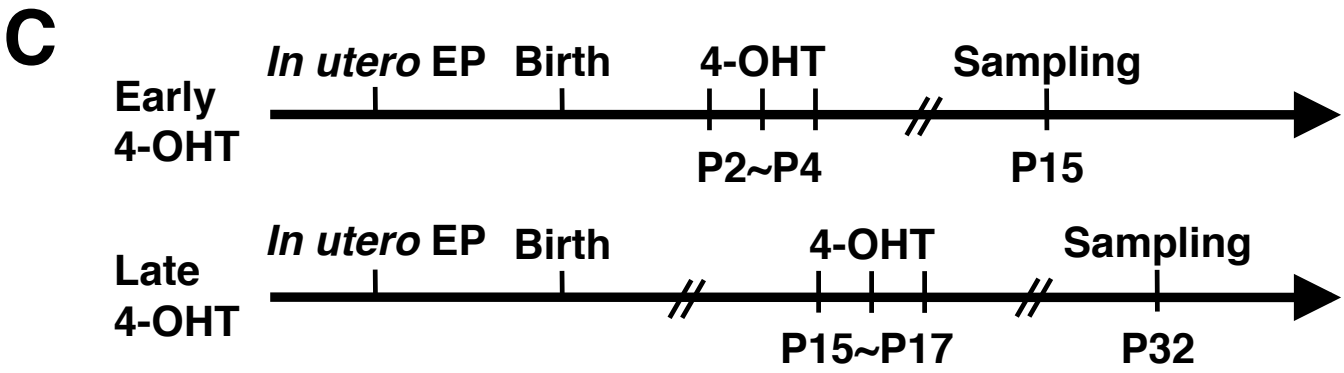

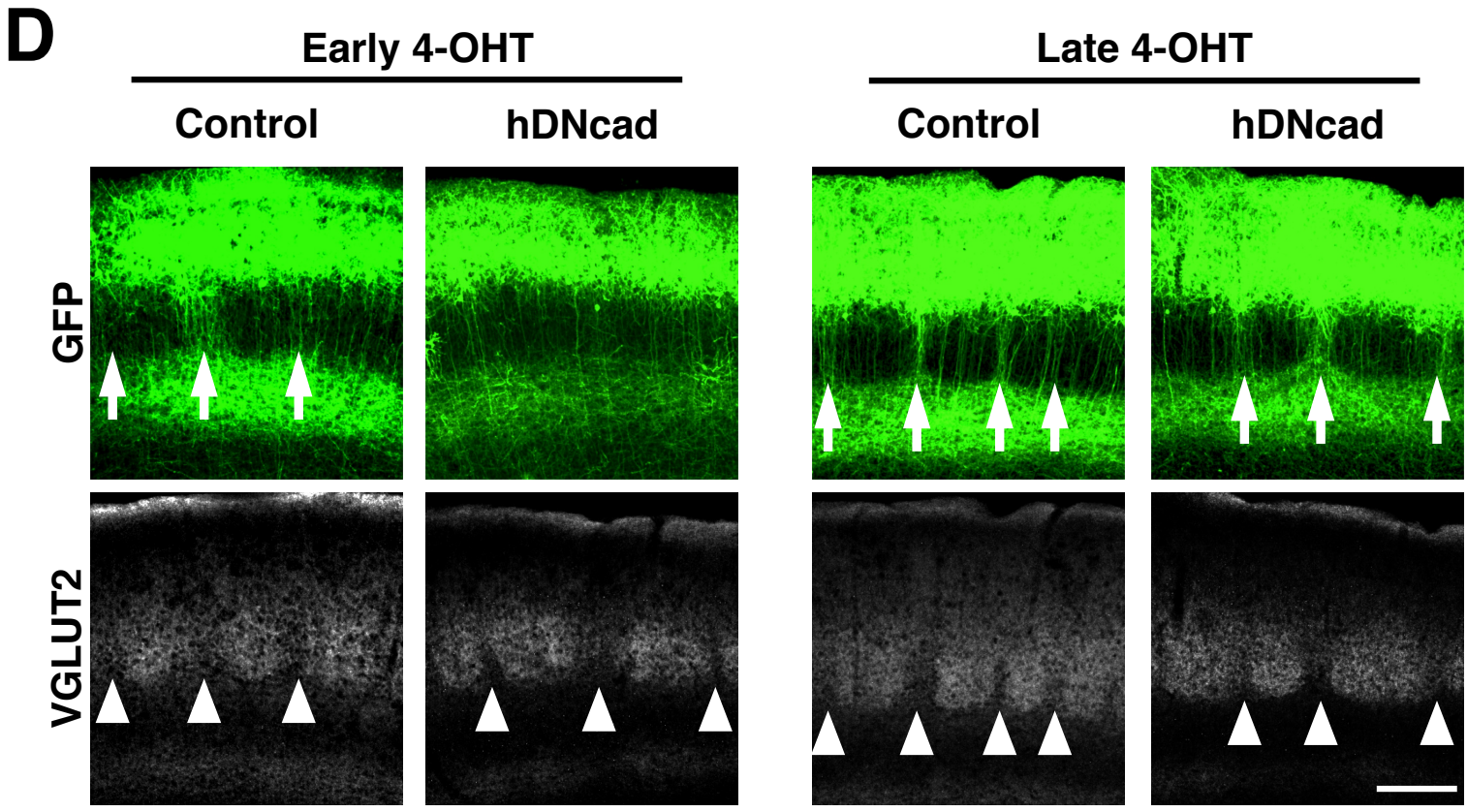

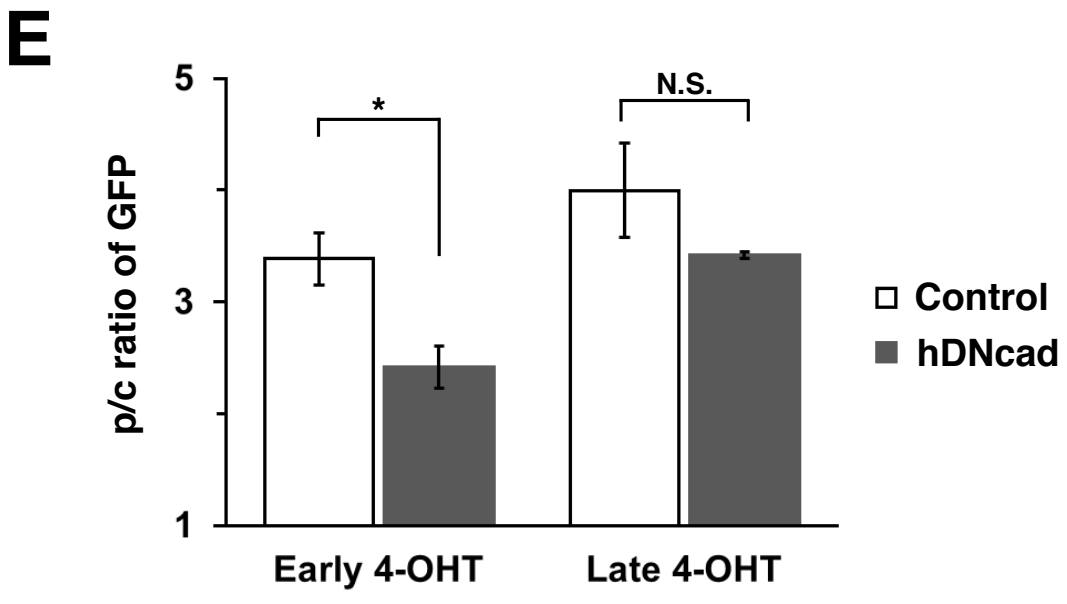

(Figure 13. continued)

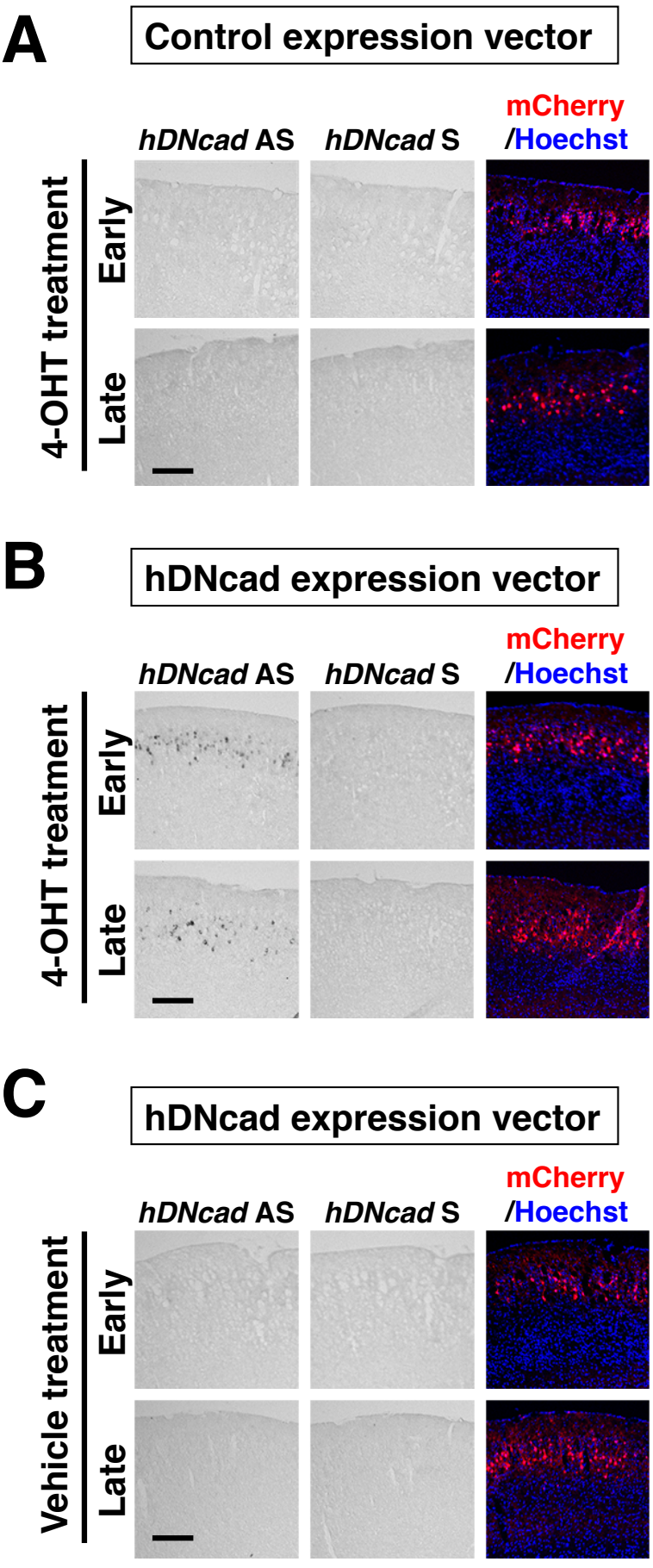

Figure 14. The expression of hDNcad in layer 2/3 neurons
Using *in utero* electroporation, pCAG-ER^{T2}CreER^{T2} and pCAG-mCherry, plus either pCAG-floxedSTOP-hDNcad or pCAG-floxedSTOP control plasmid were co-transfected at E15.5. Pups were treated with 4-OHT or vehicle at P2-4 (early) or P15-17 (late), and coronal sections of 14 μm thickness were prepared two weeks later. *In situ* hybridization using sense or antisense probe against hDNcad was performed. When the control plasmid was transfected, hDNcad probes did not show any apparent signals (*A*), suggesting that hDNcad probes do not react with endogenous mouse cadherins. In pups transfected with pCAG-floxedSTOP-hDNcad, the hDNcad antisense (AS) probe gave strong signals in both early and late 4-OHT-treated samples (*B*), whereas it did not give any signal with vehicle injection (*C*). The hDNcad sense (S) probe did not give any apparent signal (middle panels). Scale bars = 200 μm.

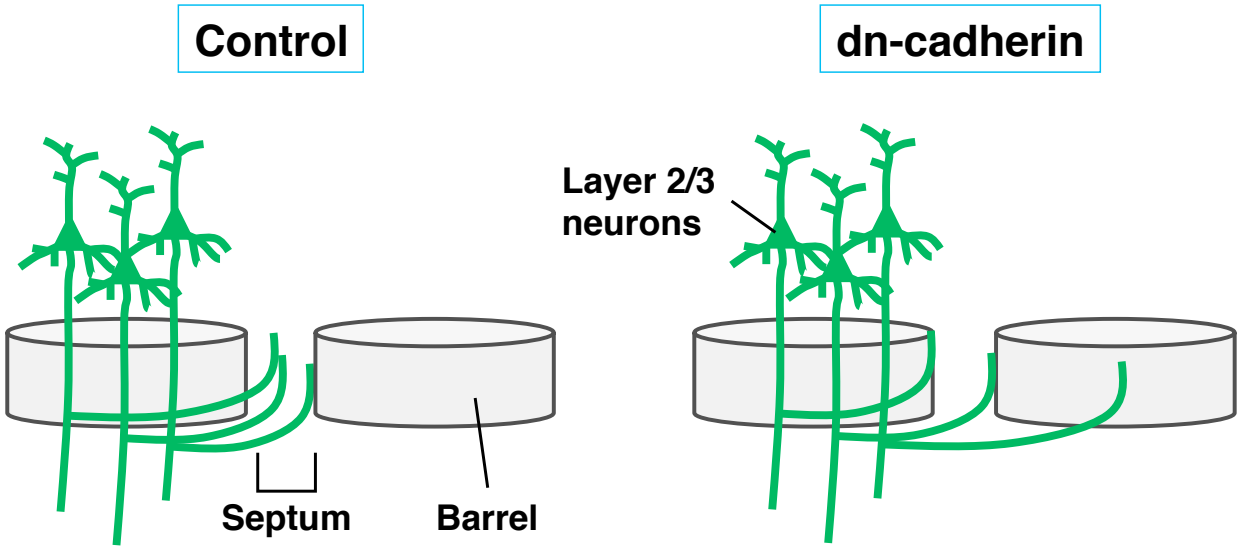

Figure 15. A hypothetical model for the role of cadherins in barrel net formation

I conclude that classic cadherins are important for barrel net formation, presumably by regulating the spatial distribution of axons of layer 2/3 neurons. Under control conditions, axons of layer 2/3 neurons interact with their targets in septal regions through homophilic binding of classic cadherins, and thus they accumulate in spetal regions. When dn-cadherin is expressed in layer 2/3 neurons, the axons fail to recognize their targets and to accumulate in septal regions of layer 4.